Pharmacological Research 213 (2025) 107652

Contents lists available at ScienceDirect

Pharmacological Research

journal homepage: www.elsevier.com/locate/yphrs

Neuronal PCSK9 regulates cognitive performances via the modulation of ApoER2 synaptic localization

Silvia Pelucchi [a,1], Lorenzo Da Dalt [a,1], Giulia De Cesare [a,1], Ramona Stringhi [a], Laura D'Andrea [a], Filippo La Greca [a], Clara Cambria [b], Lina Vandermeulen [a], Elisa Zianni [a], Stefano Musardo [a], Silvia Roda [a], Fabrizia Bonacina [a], Sofia Nasini [c], Maria Giovanna Lupo [d], Nicola Ferri [d,e], Stefano Comai [c,f,g,h], Fabrizio Gardoni [a], Flavia Antonucci [b,i], Diego Scheggia [a], Monica Di Luca [a], Giuseppe Danilo Norata [a,*,2], Elena Marcello [a,**,2]

[a] Department of Pharmacological and Biomolecular Sciences "Rodolfo Paoletti", Università degli Studi di Milano, Milan, Italy
[b] Department of Medical Biotechnology and Translational Medicine (BIOMETRA), Università degli Studi di Milano, Milan, Italy
[c] Department of Pharmaceutical and Pharmacological Sciences, University of Padua, Padua, Italy
[d] Department of Medicine, University of Padua, Padua, Italy
[e] VIMM, Veneto Institute of Molecular Medicine, Padua, Italy
[f] Department of Biomedical Sciences, University of Padua, Padua, Italy
[g] Department of Psychiatry, McGill University, Montreal, QC, Canada
[h] IRCSS San Raffaele Scientific Institute, Milan, Italy
[i] Institute of Neuroscience, IN-CNR, Milano, Italy

ARTICLE INFO

Keywords:
PCSK9
Cholesterol
Hippocampus
Spine
Synaptic plasticity
ApoER2
Lipid droplets

ABSTRACT

PCSK9 promotes the degradation of the low-density lipoprotein receptors and its inhibition by monoclonal antibodies or gene silencing approaches results in the reduction of plasma cholesterol levels coupled to that of cardiovascular events. Notably, while the liver is the primary source of circulating PCSK9, this protein is also abundantly expressed in the brain. However, its specific functions in the brain remain poorly understood. Here, we demonstrate that neuron-specific PCSK9 knockout mice exhibit impaired cognitive function, driven by alterations in hippocampal synapse morphology and synaptic plasticity mechanisms, coupled to spatial memory deficits. Among PCSK9 targets, we identified ApoER2 as the primary mediator of PCSK9-dependent effects on synaptic function. In neuronal cultures, PCSK9 downregulation affects ApoER2 synaptic membrane localization and lipid droplets abundance. In conclusion, our results highlight the critical role of neuronal PCSK9 in modulating synaptic ApoER2 and reveal the detrimental effects of its deficiency on synaptic function and cognitive performance. Our results shed light on the complex biology of PCSK9, crucial for evaluating side effects of PCSK9 inhibition and for developing new therapies targeting PCSK9 for brain disorders.

1. Introduction

The brain is the body's most cholesterol-rich organ and cholesterol homeostasis is essential for brain function [1]. The dysregulation of these complex homeostatic mechanisms in the brain can affect neuronal activity and synaptic neurotransmission, impairing vesicle exocytosis and inducing both dendrite degeneration and synaptic dysfunction [2–4]. Thus, the impairment of cholesterol metabolism represents a risk factor for the development of brain disorders such as Alzheimer's disease (AD) and major depression [5].

Cholesterol has a relatively long half-life, and brain cholesterol metabolism is largely separated from the process in peripheral tissues by the blood-brain barrier [6]. Growing evidence shows that cholesterol transport and metabolism in neurons are tightly linked to learning and

* Correspondence to: Department of Pharmacological and Biomolecular Sciences "Rodolfo Paoletti", University of Milan, Via Balzaretti 9, Milan 20133, Italy.
** Corresponding author.
E-mail addresses: danilo.norata@unimi.it (G.D. Norata), elena.marcello@unimi.it (E. Marcello).
[1] These authors are the co-first authors
[2] These authors are the co-senior and co-corresponding authors.

https://doi.org/10.1016/j.phrs.2025.107652
Received 20 December 2024; Received in revised form 7 February 2025; Accepted 11 February 2025
Available online 12 February 2025
1043-6618/© 2025 The Authors. Published by Elsevier Ltd. This is an open access article under the CC BY license (http://creativecommons.org/licenses/by/4.0/).

memory [1]. In the adult brain, cholesterol is predominantly synthesized via the mevalonate pathway in glial cells, primarily astrocytes [7,8], and then released by ATP-binding cassette transporters (ABCs) and loaded onto apolipoprotein E (ApoE). Genetic deficiency of ApoE results in a reduction of synapse numbers that is at least partially due to the loss of astrocyte-derived particles [9]. Secreted lipidated ApoE particles are taken up by neurons via receptor-mediated endocytosis [1]. Studies have shown that in the brain, ApoE binds to numerous receptors of the low-density lipoprotein receptor (LDLR) family [1], including LDLR, LRP1, and ApoER2. These receptors play various roles outside of lipid trafficking and metabolism, including synaptic transmission and modulation of spine structure [10,11].

A master regulator of the half-life of the LDLRs, particularly LDLR, is the proprotein convertase subtilisin/kexin type9 (PCSK9). Although PCSK9 was first identified in the brain, it emerged as a target for body-wide cholesterol-lowering drug development [12–15]. PCSK9 is an enzyme mainly expressed by the liver [16]. Once secreted in plasma, PCSK9 binds to LDLRs at the surface of hepatocytes, enhancing their degradation in endosomes/lysosomes and preventing their recycling [16]. This results in reduced low-density lipoprotein cholesterol (LDL-C) clearance and hypercholesterolaemia [17]. Furthermore, genetic variations in the *PCSK9* gene reliably alter the regulation of hypercholesterolemia [18,19]. These data underscore the role of PCSK9 as an important regulator of LDL-C. Consequently, monoclonal antibodies inhibiting PCSK9 as well gene silencing approaches were developed to reduce LDL-C levels. These approaches are effective in reducing LDL-C by as much as 50 %–60 %, providing considerable cardiovascular benefit [20–22].

Despite the well-known role of PCSK9 in hepatic lipoprotein metabolism, there is emerging evidence for its involvement in different biological pathways, relating to pancreatic and cardiac function [23,24]. Moreover, in the brain, PCSK9 appears to be relevant for neuronal differentiation as well as for the activation of astrocytes and microglia. Indeed, PCSK9 is highly expressed in the embryonic brain telencephalon and is implicated in the differentiation of neural progenitor cells to neurons [25]. PCSK9 also regulates apoptosis and its proapoptotic signaling is mediated by altered ApoER2 function [26]. PCSK9 downregulates LDLR levels during brain development and following transient ischemic stroke in adult mice [27]. However, *in vitro* and *in vivo* studies in adult mice offer contradictory evidence regarding whether PCSK9 in the brain targets LDLR, VLDLR, and ApoER2 for degradation. In heterologous cells, PCSK9 transfection resulted in a substantial decrease in all three receptor protein levels [28], while $PCSK9^{-/-}$ adult mice did not have significantly different levels of LDLR [27,29]. In addition, PCSK9 overexpression or deletion did not affect LDLR, VLDLR, or ApoER2 levels in the hippocampus and cortex of the adult mouse brain [29].

On the other hand, neural PCSK9 expression is reportedly upregulated in adult brains during disease states, including AD, alcohol use disorder, ischemic stroke, and neuropsychiatric disorders [30]. For instance, PCSK9 concentrations are increased in the cerebral spinal fluid (CSF) of AD patients and other neurodegenerative diseases [31,32]. However, pathophysiological studies on preclinical models of AD are yet to determine the potential role of PCSK9 in the disease pathogenesis [33].

Overall, preclinical studies have so far implicated PCSK9 in both healthy brain physiology and pathological conditions. However, its exact role in neurons still needs to be clarified.

Clinical studies with monoclonal antibodies have excluded an impact of the inhibition of circulating PCSK9 and the subsequent hypocholesterolemia on cognition [33–35], confirming the distinction between brain and systemic cholesterol metabolism. Nevertheless, the observation that the brain is the second largest PCSK9-producing organ, coupled with the preclinical evidence summarized above, suggests that the protein could indeed play a role in neuronal function.

Here, we show that the lack of PCSK9 causes impairment of cognitive function and synaptic plasticity pathways in systemic $PCSK9^{-/-}$ mice. To clarify the specific role of neuronal PCSK9, we generated a new transgenic line selectively lacking PCSK9 in neuronal cells. In this experimental model, we observed that PCSK9 deficiency impairs spatial memory and affects spine morphology, synaptic localization of glutamate receptors, and synaptic pathways in the hippocampus. Notably, we found that ApoER2 is the primary target of PCSK9 in neurons. Experiments performed in primary hippocampal cultures revealed that PCSK9 downregulation affects ApoER2 synaptic membrane expression and lipid droplet levels.

These results highlight the relevance of PCSK9 in brain physiology through its ability to control synaptic structure and function.

2. Materials and methods

2.1. Animal care

All procedures involving the preparation of primary hippocampal cultures were conducted in accordance with the ethical standards of the Institutional Animal Care and Use Committee of the University of Milan (Italian Ministry of Health permit #5247B.N.YCK/2018). Sprague–Dawley pregnant rats were purchased from Charles River Laboratories (Calco, Italy). Embryos were used at embryonic day 19 to prepare hippocampal neuronal cultures. Animals in all procedures were maintained in cages with free access to food and water in a controlled environment with a 12 h/12 h light/dark cycle and a controlled temperature of 22°C.

B6;129Sv-Pcsk9tm1Jdh/J male mice from the Jackson Laboratory (Bar Harbor, ME, USA) were backcrossed to C57Bl6J females for more than 10 generations. Heterozygous mutant mice from the F10 generation were intercrossed to generate littermate WT and KO mice. B6.Cg-Tg (Alb-cre)21Mgn/J male mice from the Jackson Laboratory (Bar Harbor, ME, USA) were backcrossed to Pcsk9LoxP/LoxP females (provided by Merck Research Laboratories) for 10 generations. Heterozygous mutant mice from the F10 generation were intercrossed to generate littermate AlbCre-/Pcsk9LoxP/LoxP and AlbCre+ /Pcsk9LoxP/LoxP mice which were treated as previously described. B6.Cg-Tg(Camk2α-cre)T29–1Stl/J male mice from the Jackson Laboratory (Bar Harbor, ME, USA) were backcrossed with $PCSK9^{fl/fl}$ females (provided by Merck Research Laboratories) for 5 generations [36]. Hemizygous mutant mice from the F5 generation were intercrossed to generate littermate CaMKIIα Cre^{+}/$PCSK9^{fl/fl}$ and CaMKIIα Cre^{-}/$PCSK9^{fl/fl}$ mice. The mice were kept under controlled light/dark cycle (12 hours of light/12 hours of dark) and temperature-controlled conditions (21°C). They had free access to food and water. Starting at 8 weeks of age and for 20 weeks, mice were fed with a Standard Fat Diet (SFD). Both male and female animals were used for experimental procedures. All the experimental procedures were approved by local authorities (Ministero della Salute, IT, Aut. Min. 580/2019, 428/2021, and 178/2024-PR) and complied with the WMA Statement on animal use in biomedical research and the EU recommendations (Directive 2010/63/EU) for experimental design and analysis in pharmacology care.

2.2. Recognition memory tests

The procedures for recognition and object location tasks involved an acquisition/sample phase (5 min) and a recognition test (5 min), separated by a 2- or 24-hour delay. After acquisition, all objects were cleaned with alcohol to remove olfactory cues and any sawdust that had stuck to the object. The objects were constructed from Duplo blocks (Lego), varied in shape, color, and size, and were too heavy to be displaced. Mice were tested in a standard open field arena (UgoBasile, 44 × 44 cm) with black PVC walls. A digital camera (Imaging Source, DMK 22AUC03 monochrome) was placed above the apparatus to record the test using a behavioral tracking system (Anymaze 6.0, Stoelting). These videos were used offline by experimenters who were blind to the genotypes for a posteriori scoring of the time spent in the different zones of the

apparatus and exploratory behavior, defined as the animal directing its nose toward an object at a distance of at least 2 cm. To express the discrimination between the objects we calculated a discrimination index as the absolute difference in the time spent exploring the novel or displaced objects and the familiar objects divided by the total time spent exploring the objects. All mice were habituated to the open field arena for 15 minutes the day before testing. Animals that failed to complete a minimum of 10 s of exploration in the test phase were excluded from the analysis. In the acquisition phase, two identical objects were placed near the corners of one wall in the arena (10 cm from the walls). The animals were placed into the arena and allowed to explore for 5 min. During the test, one of the two objects was replaced with a novel object (novel object recognition task) or displaced to the corner adjacent to its original position, such that the two objects were diagonal from each other (object location task). The positions of the objects in the test (familiar or displaced) and the objects used as novel or familiar were counterbalanced between the animals.

2.3. Open field test

Mice were individually placed in a corner of an open field arena (UgoBasile, 44 × 44 cm) with black PVC walls and left free to explore it for 20 minutes. The test was recorded by a camera placed above the apparatus, and the distance traveled by the animals was measured using the behavioral tracking software Anymaze 6.0 (Stoelting).

2.4. Rotarod test

Motor coordination was evaluated using the rotarod apparatus. Over three consecutive days, mice underwent training on a rotarod device (Ugo Basile, Comerio, VA, Italy) set at a constant speed of 15 rpm for 5 minutes. If mice fell, they

were promptly placed back onto the rotating rod. On the fourth day, mice were placed on the rotating rod set to a speed of 28 rpm, and the latency to fall from the device or to cling and rotate for two full rotations was recorded. Subsequently, mice underwent two additional trials with a minimum interval of 5 minutes to rest between each trial. The best performance from the three trials was used for the analysis.

2.5. Dendritic spine labeling

Carbocyanine dye DiI (ThermoFisher) was used to label neurons [37]. DiI crystals were applied using a thin needle by delicately touching the region of interest on both sides of 2 mm coronal sections prepared from brains fixed by intra-cardiac perfusion with 1.5 % Paraformaldehyde (PFA) in 0.1 M phosphate buffer (PB) (animals were anesthetized by intraperitoneal injection of Ketamine 10 mg/kg and Xilazine 0.75 mg/Kg). DiI was left to diffuse for 1 day in the dark at room temperature before sections were fixed again with 4 % PFA in PB 0.1 M for 45 min at 4 °C. 150 μm coronal sections were then obtained using a vibratome, with the first section being discarded. Sections were mounted on glass slides with Fluoromount mounting medium (Sigma-Aldrich) for confocal imaging.

2.6. PCSK9 ELISA

PCSK9 concentration was measured by ELISA (R&D System, cat. n. MPC900) according to manufacturer instructions in cortical, hippocampal, liver extract, and plasma samples. Cortical and hippocampal samples were lysed at 4°C in an ice-cold buffer with Roche cOmplete™ Protease Inhibitor Cocktail, Ser/Thr and Tyr phosphatase inhibitors (Sigma-Aldrich), 0.32 M Sucrose, 1 mM Hepes, 1 mM NaF, 0.1 mM PMSF, 1 mM $MgCl_2$ using a glass-Teflon homogenizer. Total protein extracts from the liver were obtained by lysing 10 mg of tissue with 100 μl of RIPA buffer containing a cocktail of protease and phosphatase inhibitors (Roche Diagnostics). Blood samples were collected from cardiac puncture on EDTA and plasma was collected following centrifugation for 10 minutes at 3000 rpm.

2.7. Triton-insoluble fraction postsynaptic membrane preparation

Triton insoluble fraction (TIF), a fraction highly rich in all categories of postsynaptic density proteins (i.e. receptor, signaling, scaffolding, and cytoskeletal elements) absent of presynaptic markers [38], was obtained from CaMKIIα Cre^{+}/$PCSK9^{fl/fl}$ and CaMKIIα Cre^{-}/$PCSK9^{fl/fl}$ hippocampal samples. Hippocampi were homogenized at 4°C in an ice-cold buffer with Roche cOmplete™ Protease Inhibitor Cocktail, Ser/Thr and Tyr phosphatase inhibitors (Sigma-Aldrich), 0.32 M Sucrose, 1 mM Hepes, 1 mM NaF, 0.1 mM PMSF, 1 mM $MgCl_2$ using a glass-Teflon homogenizer. An aliquot of homogenate (Homo) was kept for western blot (WB) analysis. Homo were then centrifuged at 1000 g for 5 minutes at 4°C to remove nuclear contamination and white matter. The supernatant was collected and centrifuged at 13,000 g for 15 minutes at 4°C. The resulting pellet (crude membrane fraction) was resuspended in resuspension buffer (1 mM Hepes with protease inhibitors (Roche cOmplete™)) and then centrifuged at 100,000 g for 1 h at 4°C. Triton-X extraction of the resulting pellet was carried out at 4°C for 15 minutes in an extraction buffer (1 % Triton-X, 75 mM KCl, and protease inhibitors (Roche cOmplete™ Protease Inhibitor Cocktail)). After extraction, the samples were centrifuged at 100,000 g for 1 h at 4°C and the TIFs obtained were resuspended in 20 mM HEPES with protease inhibitors (Roche cOmplete™ Protease Inhibitor Cocktail).

2.8. SDS-PAGE and western blot analyses

Protein samples were separated by electrophoresis onto acrylamide/bisacrylamide gel at the appropriate concentration, transferred to a nitrocellulose membrane, and probed with the corresponding primary antibody (Ab) followed by incubation with appropriate horseradish peroxidase-conjugated secondary Ab (Bio-Rad). Chemiluminescence signal was visualized using Chemidoc Imaging System and ImageLab software (Bio-Rad).

2.9. Immunoprecipitation assay

Aliquots of 15 μg of TIF obtained from CaMKIIα Cre^{+}/$PCSK9^{fl/fl}$ and CaMKIIα Cre^{-}/$PCSK9^{fl/fl}$ hippocampal homogenates were incubated with an Ab against GluN2B overnight at 4°C in a final volume of 200 μl of RIA buffer (200 mM NaCl, 10 mM ethylene-diamine-tetra-acetic acid (EDTA), 10 mM Na_2HPO_4, 0.5 % NP-40, 0.2 % sodium dodecyl sulfate (SDS)). SureBeads Protein A/G Magnetic Beads (Bio-Rad) were used to precipitate the immunocomplex; the beads were resuspended in Laemmli buffer and heated for 3 minutes before loading onto SDS-PAGE. Beads were applied onto SDS-PAGE; the precipitated immunocomplex was revealed by an Ab recognizing phosphorylated tyrosine residues (PY20 Ab). Membranes were reprobed to stain total immunoprecipitated GluN2B.

2.10. Cholesterol and triglycerides measurement in plasma and hippocampal tissue

Plasmatic level of cholesterol and triglycerides levels were measured on O/N fasted mice as previously described using a total cholesterol kit (ABX Pentra, HORIBA Medical, CH200; Cat: A11A01634) and triglycerides (ABX Pentra, HORIBA Medical, TR210; Cat: A11A01640) according to the manufacturer's instructions [39].

Cholesterol level in the hippocampus was measured after lipid extraction form tissues with the following protocol: briefly, 10 mg of hippocampus were homogenized with 1 ml of extracting solution (MeOH/ACN 1:1, v/v) using tissue lyser (max power, 1 min). Samples were centrifuged at 16,000 g for 10 minutes at 4°C, the supernatant was kept for lipid quantification while the pellet for protein quantification.

Total cholesterol level was then quantified as previously reported with commercially available Kit (ABX Pentra, HORIBA Medical, CH200; Cat: A11A01634) [39]. Data were normalized on total hippocampal protein content determined by Lowry assay data are expressed as μg of cholesterol /μg of protein.

2.11. Cell culture and treatments

Hippocampal primary neurons were isolated from the rat hippocampus at embryonic day 18–19 (E18–19) as previously described[40]. Stimulation of synaptic NMDA receptors was obtained by treating hippocampal neurons with 50 mM Bicuculline (Tocris), 2.5 mM 4-AP, and 5 mM ifenprodil in Neurobasal medium supplemented with B27[41]. Transfection with calcium phosphate was performed at 10 days in vitro (DIV) and analyses were conducted at DIV15.

COS7 cells were purchased from ATCC and maintained in DMEM containing Glutamax (Gibco) supplemented with 10 % fetal bovine serum and penicillin-streptomycin (Gibco). At passage 10–15, cells were transfected using the lipofectamine LTX (Thermo Fisher). After 24 h, COS-7 cells were processed for biochemical analysis.

2.12. Plasmids

The retroviral expression plasmid encoding PCSK9-FLAG tag was constructed using the pBMN-IRES-PURO plasmid. To knock down PCSK9 expression, the shRNA sequence GCCTGGAGTTTATTCGGAAGA [42] was cloned in the vector pAAV-U6 >CaMKIIprom>mCherry, which expresses the mCherry fluorescent protein under the control of the neuron-specific promoter CaMKII (shPCSK9). A scramble control sequence was cloned in the same vector (GCACTACCAGAGCTAACTCAGATAGTACT) and used as a negative control (SCR). The same sequences were cloned in a vector expressing GFP, under the control of CMV promoter, as the reporter gene.

2.13. Immunofluorescence

For co-localization and morphological studies, DIV15 primary hippocampal neurons were fixed in 4 % PFA supplemented with 4 % sucrose in Dulbecco's phosphate-buffered saline (PBS) solution, permeabilized with Triton 0.1 % in PBS, and blocked with 5 % bovine serum albumin (BSA). Primary Ab incubation was performed overnight at 4°C. The specific Abs used are listed in the antibodies section. After washes with PBS, secondary Abs (Alexa Fluor, Thermo Fisher) were added, and samples were incubated for 1 h at room temperature. Coverslips were mounted with Fluoroshield (Sigma, cat number F6182).

To evaluate surface and total staining, transfected neurons were fixed with 4 % PFA, 4 % sucrose in PBS pH 7.4, and then incubated with an ApoER2 Ab. To visualize surface expression, cells were then blocked with 4 % normal serum, followed by a 488-conjugated secondary Ab. Afterward, cells were permeabilized with 0.1 % Triton X-100 for 12 minutes and intracellular expression was determined by incubating cells with the ApoER2 Ab and labeling the total receptor fraction with a 647-conjugated secondary Ab.

To stain lipid droplets, transfected hippocampal neurons were washed 3 times in PBS, fixed in 4 % PFA, and stained with 1 μg/ml Nile Red (Thermo Fisher Scientific, cat number N1142) for 10 minutes at room temperature. Images were acquired using confocal microscopy.

2.14. Confocal microscopy

Images were acquired with the Zeiss confocal laser scanning microscope LSM900 as a z-stack series (except for colocalization analysis), using a 63X oil immersion objective. For Sholl analysis, we used a 40X oil immersion objective with a zoom of 0.7X. Images were acquired using a Plan-Apochromat 63x/NA 1.4 Oil M27 objective.

For ApoER2-PSD95 colocalization experiments, images were taken in super-resolution modality using an LSM900 confocal microscope with the Airyscan detector (Carl Zeiss) and equipped with a 63X oil immersion objective.

2.15. RNA extraction and RT-qPCR

RNA was extracted from DIV15 neurons in TRIZOL (Thermo Fisher) according to the supplier's specifications. RT-qPCR was performed with the iTaq Universal SYBR Green One-Step Kit (Bio-Rad, 1725151) using the CFX-384 well plate instrument (Bio-Rad).

The following oligos were used for qPCR analysis:

Rat *LDLR* (Fw: GTGTGACCGTGAACATGACTGC; Rv: CACTCCCCACTGTGACACTAGA)

Rat *LRP1* (Fw: CCTTGACCCTGACAAGCCTA; Rv: TGTAGAGCGTGGCATACACT)

Rat *LRP8* (ApoER2) (Fw: TGACTTCCAGTGTGGGGATG; Rv: CCTCACAAGTTGACTCCTGC)

Rat *ARC* (Fw: TAAGCGGGACCTGTACCAGA; Rv: GGTGCCCACCACATACTGAA)

Rat HISTONE H3 (Fw: CGTTGGAGGAGCTTCGTCTT; Rv: GGCCATCTTCTCTCACCCAA-3′

Rat *TUBULIN A1A* (Fw: CGCTGTAAGAAGCAACACCTC;

Rv: ACACTCACGCATGGTTGCTG)

2.16. In vitro electrophysiology

Whole-cell patch-clamp recordings were obtained from shPCSK9-transfected neurons and relative controls at DIV13–14 in the voltage-clamp modality using the Axopatch 200B amplifier and the pClamp-10 software (Axon Instruments). Recordings were performed using the Krebs'-Ringer's-HEPES (KRH) external solution prepared as follows: NaCl 125 mM, KCl 5 mM, $MgSO_4$ 1.2 mM, KH2PO4 1.2 mM, $CaCl_2$ 2 mM, glucose 6 mM, HEPES-NaOH pH 7.4 25 mM). Recording pipettes were fabricated from glass capillaries (World Precision Instruments) using a two-stage puller (Narishige). Capillaries were filled with the intracellular solution potassium-gluconate (KGluc 130 mM, KCl 10 mM, EGTA 1 mM, HEPES 10 mM, $MgCl_2$ 2 mM, MgATP 4 mM, GTP 0.3 mM) and the tip resistance was about 3–5 MW. To identify mEPSCs, neurons were held at −70 mV, and Tetrodotoxin (TTX) 1 mM was added to the external solution. Finally, the analysis was performed using Clapfit-pClamp 10 software, after choosing an appropriate standard threshold.

2.17. Antibodies

The following primary Abs were used: anti CREB (Millipore, Cat. AB3006), anti p-CREB (Millipore, Cat. 06519), ERK1/2 (Cell Signalling Cat. 9102), anti-pERK1/2 (Cell Signalling Cat. 9101), GluN1 (Invitrogen Cat. 320500), GluN2A (Invitrogen Cat. 480031), GluN2B (Cell Signalling Cat. N.14544 s), GluA1 (AbCaM Cat. ab31232), GluA1p845 (AbCaM Cat. ab76321), ApoER2 (Invitrogen MA5–36130), VLDLR (Abcam, cat. ab302917), LDLR (Proteintech, cat. 10785–1-AP), LRP1 (AbCaM Cat. Ab92544), PSD-95 (AbCaM Cat. 192757; Cell Signalling Cat. 3450S), GFP (Neuromab Cat. 525295), pY20 (Calbiochem Cat. 525295), pGluN2BTyr1472 (Biorad Cat. N. AHP1004), FLAG (Sigma-Aldrich Cat. F7425), anti-Tubulin (Sigma-Aldrich, cod. T9026), anti-RFP (Clontech, cod. 632496).

The Alexa Fluor dye secondary antibodies used were purchased from Thermo Fisher Scientific. The peroxidase-conjugated secondary antibodies were purchased from Bio-Rad.

2.18. Quantification and statistical analysis

To minimize the possibility of bias in experimental results, randomization, and blinding were used in experimental design, imaging acquisition, and analyses. Cell cultures with viability lower than 80 % were excluded from the analyses.

Acquisition and quantification of western blotting were performed using computer-assisted imaging (ChemiDoc system and Image lab 4.0 software; Bio-Rad). Data obtained by coimmunoprecipitation assays were normalized to the amount of immunoprecipitated protein.

For imaging experiments, all the images were processed with Fiji software (US National Institutes of Health). In the representative images background neurons have been excluded. For the analysis of spine density and morphology, z-stack acquisitions were analyzed using ImageJ free software, and spine length, head width, and neck width were measured for each spine with the straight line function.

For each dendritic spine, the measures of length, head, and neck width were used to classify spines into three categories (thin, stubby, or

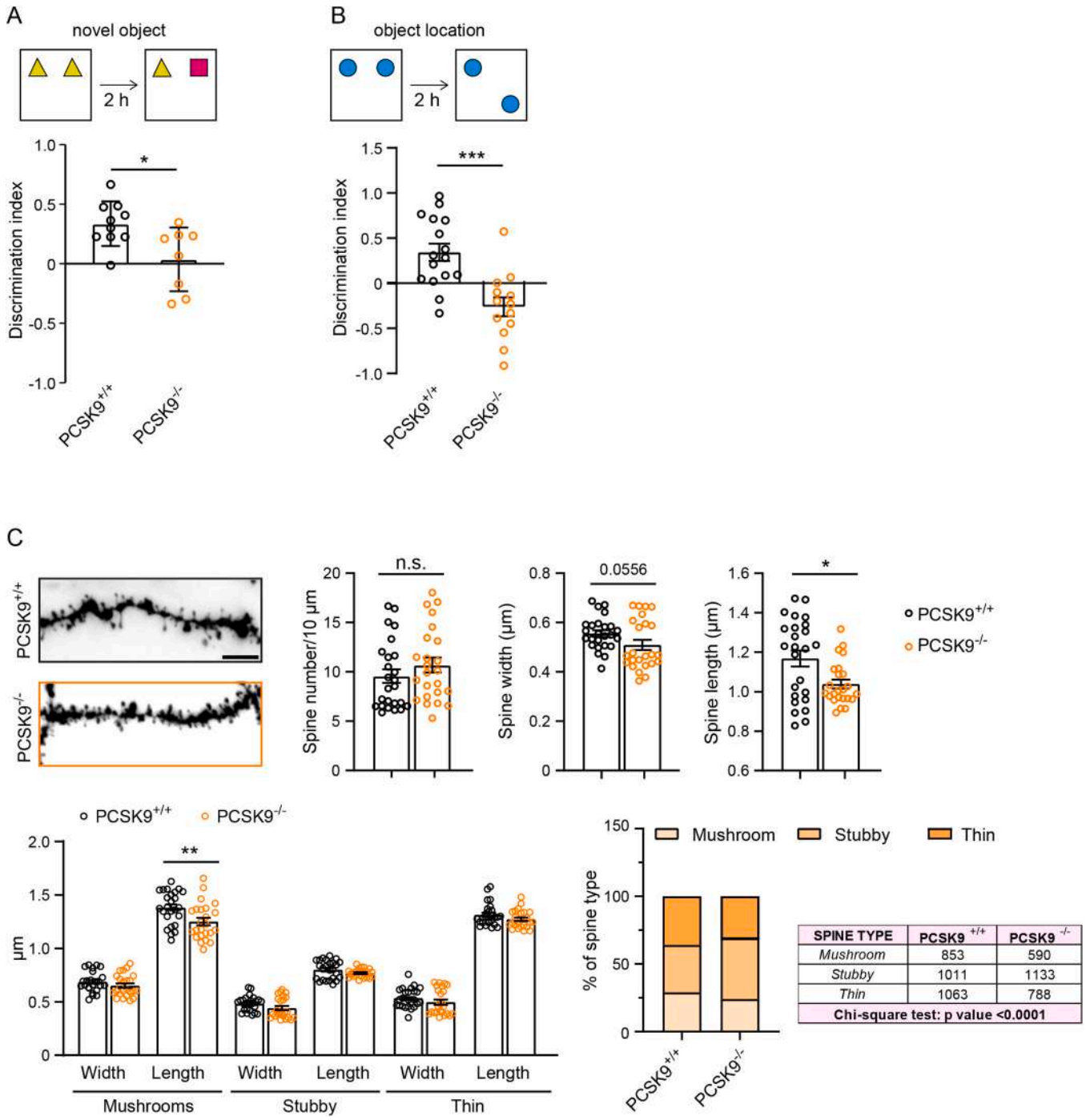

SPINE TYPE	PCSK9 +/+	PCSK9 -/-
Mushroom	853	590
Stubby	1011	1133
Thin	1063	788
Chi-square test: p value <0.0001		

Fig. 1. Cognitive deficits and dendritic spine alterations in PCSK9$^{-/-}$ mice. A. Top, schematic representation of the novel object recognition test. Bottom, discrimination index of PCSK9$^{-/-}$ (n = 8) and PCSK9$^{+/+}$ (n = 10) mice in the object recognition task 2 h after the sample phase (two-tailed unpaired *t*-test, t = 2.96, df=16, * P = 0.0130). B. Top, schematic representation of the novel object location test. Bottom, discrimination index of PCSK9$^{-/-}$ (n = 13) and PCSK9$^{+/+}$ (n = 16) mice in the object location recognition task 2 h after the sample phase (two-tailed unpaired *t*-test, t = 4.230, df=27, *** P = 0.0002). C. Left, representative confocal images of hippocampal spines from PCSK9$^{+/+}$ and PCSK9 $^{-/-}$ mice. Scale bar: 5 µm. Right, quantification of hippocampal spine density, spine head width, and spine length of PCSK9$^{+/+}$ and PCSK9 $^{-/-}$ mice (PCSK9$^{+/+}$, n = 25 neurons from 4 mice, PCSK9$^{-/-}$, n = 24 neurons from 4 mice; spine length, Mann Whitney test, * P = 0.034). Below, the analysis of dendritic spine type distribution, and spine width and length are reported (mushroom spine length: two-tailed unpaired *t*-test, t = 2.787, df = 47, ** P = 0.0076; Chi-squared test p < 0.0001). In all figures, values are expressed as mean ± SEM.

mushroom) [38]. Sholl analysis and the measurement of total dendritic length were performed on transfected neurons using the Neuroanatomy plug-in of the Fiji freeware software [40]. The Sholl interval was set at 5 μm. Colocalization analysis was performed using the JACoB plugin (Fiji software), and results were expressed considering Manders' coefficient.

Statistical analyses were performed using GraphPad Prism (version 9.3). G Power Software was used to calculate the adequate sample size. The type of parametric or non-parametric test used for each experiment, the corresponding p-values, and the type of adjustment for multiple comparisons (if any) are provided in figure legends. All statistical tests were two-sided and results were considered statistically significant if $P < 0.05$.

3. Results

3.1. Systemic deletion of PCSK9 impairs hippocampal function

To investigate whether the role of PCSK9 in systemic and cellular lipid and lipoprotein metabolism might affect cognitive function, we characterized PCSK9$^{-/-}$ mice using a battery of behavioral tests.

As an initial screening tool to assess general cognitive and behavioral performance, we tested PCSK9$^{-/-}$ and PCSK9$^{+/+}$ (wild-type) mice in the novel object recognition task, where the relative familiarity of an object is used to judge memory of prior encounters. Mice were presented with a pair of identical objects and after a 2-hour delay, one of the two was replaced with a novel object. We then calculated a discrimination index, with positive values indicating increased exploration of the novel over the familiar object. PCSK9$^{-/-}$ mice showed significantly worse performance compared to PCSK9$^{+/+}$ animals (Fig. 1A); while PCSK9$^{+/+}$ mice spent more time exploring the novel object than the familiar one, PCSK9$^{-/-}$ mice were unable to distinguish the two. We next tested a different type of recognition memory involving information about where an object had been previously encountered. To do this, we used the object location recognition memory task (Fig. 1B), which specifically engages hippocampal circuits [43]. The mice were presented with two objects, and following a 2-hour delay, one of the objects exchanged position. In this task, PCSK9$^{-/-}$ mice also failed to discriminate between the displaced and familiar objects (Fig. 1B). Together, this suggests that PCSK9 systemic deletion in mice impacts cognitive function. We did not observe any locomotor impairment, as measured in the open field and rotarod tests (Suppl. Fig. 1A).

Given that the object location recognition memory is known to be hippocampus-dependent [43], we analyzed spine morphology on Carbocyanine dye DiI-stained hippocampal slices of PCSK9$^{-/-}$ and PCSK9$^{+/+}$ mice. Hippocampal neurons of PCSK9$^{-/-}$ mice showed a significant reduction in spine length and a tendency towards decreased spine head width, while no changes in spine density were detected (Fig. 1C). Evaluation of spine shape revealed that different spine categories (mushroom, stubby, thin, filopodia) were associated with PCSK9 genetic deletion (Fig. 1C, chi-square test, $p < 0.0001$). PCSK9$^{-/-}$ mice show an increased proportion of stubby spines and a concomitant reduction of mature mushroom spines. Furthermore, mushroom spines of PCSK9$^{-/-}$ mice show a reduced spine length when compared to the mushroom spines of PCSK9$^{+/+}$ animals (Fig. 1C). Overall, these data support the hypothesis that the loss of PCSK9 negatively affects hippocampal function.

3.2. Deletion of PCSK9 in neurons impairs hippocampal-dependent cognitive function

Considering the effect of systemic PCSK9 absence on hippocampal dendritic spine morphology, we decided to investigate the consequences of the specific deletion of neuronal PCSK9 on brain function. To this aim, we generated transgenic mice selectively lacking PCSK9 production in Ca^{2+}-calmodulin kinase IIα (CaMKIIα)-expressing neurons, found predominantly in the hippocampus and cortex [44,45]. PCSK9$^{fl/fl}$ mice were crossed with CaMKIIα Cre mice. To assess the specificity of PCSK9 deletion we performed ELISA to measure PCSK9 concentrations in the liver, plasma, cortex, and hippocampus of CaMKIIα Cre^{+}/PCSK9$^{fl/fl}$ mice and corresponding controls (CaMKIIα Cre^{-}/PCSK9$^{fl/fl}$).

As shown in Fig. 2A, PCSK9 levels were significantly reduced in both the hippocampus and cortex of CaMKIIα Cre^{+}/PCSK9$^{fl/fl}$ mice compared to controls, but not in the liver or plasma. Accordingly, circulating total cholesterol and triglycerides were not different in the plasma of CaMKIIα Cre^{+}/PCSK9$^{fl/fl}$ mice (Suppl. Fig. 2A). To confirm the specificity of the assay, we also measured hippocampal PCSK9 concentration in mice selectively lacking PCSK9 production in the liver (AlbCre^{+}/PCSK9$^{fl/fl}$ mice) and therefore deficient for PCSK9 only in the circulation [24]. As expected, hippocampal PCSK9 levels are not affected in such mice compared to their controls (AlbCre^{-}/PCSK9$^{fl/fl}$), thus confirming the specificity of our results.

Based on our results on PCSK9$^{-/-}$ mice, we focused on hippocampal-dependent cognitive functions, and so tested CaMKIIα Cre^{+}/PCSK9$^{fl/fl}$ and control mice in the object location recognition memory task. While control mice preferred to explore the displaced object, CaMKIIα Cre^{+}/PCSK9$^{fl/fl}$ explored both familiar and displaced objects equally, suggesting a lack of distinction (Fig. 2B). With a longer delay between sample and test phases, CaMKIIα Cre^{+}/PCSK9$^{fl/fl}$ continued to exhibit a lower discrimination index compared to control mice (Fig. 2C). Altogether these results suggest that genetic deletion of neuronal PCSK9$^{fl/fl}$ has an impact on hippocampal-dependent cognitive functions.

3.3. Neuronal deletion of PCSK9 in mice affects hippocampal synapses

Considering the results of behavioral tests, we investigated the morphology of the spines in the hippocampus of CaMKIIα Cre^{+}/PCSK9$^{fl/fl}$ mice. As shown in Fig. 3A, no significant changes in spine density or morphology (width and length) were detected. Analysis of spine subtypes did however show that the PCSK9 neuronal deletion was linked to a change in the proportion of spine types (Fig. 3A, chi-square test, $p < 0.0001$). Specifically, the hippocampal neurons of CaMKIIα Cre^{+}/PCSK9$^{fl/fl}$ mice exhibit a moderately greater number of mature mushroom spines and a slight reduction in the proportion of stubby spines.

To assess molecular alterations related to synaptic function, we analyzed the cAMP-responsive element-binding protein (CREB) and extracellular signal-regulated kinase (ERK) signaling pathways which are crucial for synaptic plasticity events.

As shown in Fig. 3B, the phosphorylation of ERK was reduced in hippocampal homogenates of CaMKIIα Cre^{+}/PCSK9$^{fl/fl}$ compared to control mice, indicating that PCSK9 neuronal deletion affects ERK signaling. In addition, the analysis of CREB pathway revealed a tendency of CREB phosphorylation levels to decrease in CaMKIIα Cre^{+}/PCSK9$^{fl/fl}$ hippocampi compared to control mice.

Considering that these signaling pathways are controlled by glutamate receptors, we analyzed the molecular composition of the postsynaptic compartment. To this aim, we purified the Triton-Insoluble Fraction (TIF), which is enriched in postsynaptic proteins [38], from the hippocampi of CaMKIIα Cre^{+}/PCSK9$^{fl/fl}$ mice and corresponding controls. We analyzed N-methyl-D-aspartate receptor (NMDAR) subunits (i.e., the obligatory subunit GluN1, and GluN2A and GluN2B) and α-amino-3-hydroxy-5-methyl-4-isoxazole propionic acid receptors (AMPARs).

Even though a reduction in total GluN2A levels was detected in CaMKIIα Cre^{+}/PCSK9$^{fl/fl}$ mice compared to control animals (Fig. 4A), no changes in synaptic levels were found in the postsynaptic compartment (Fig. 4B). However, in comparison to control animals, CaMKIIα Cre^{+}/PCSK9$^{fl/fl}$ mice showed an increase in GluN1 and GluN2B synaptic abundance (Fig. 4B), indicating an enrichment of GluN2B-containing NMDARs in CaMKIIα Cre^{+}/PCSK9$^{fl/fl}$ mice synapses. This increase was observed without changes in the total GluN1 and GluN2B protein levels (Fig. 4A). No modifications in the expression or synaptic localization of

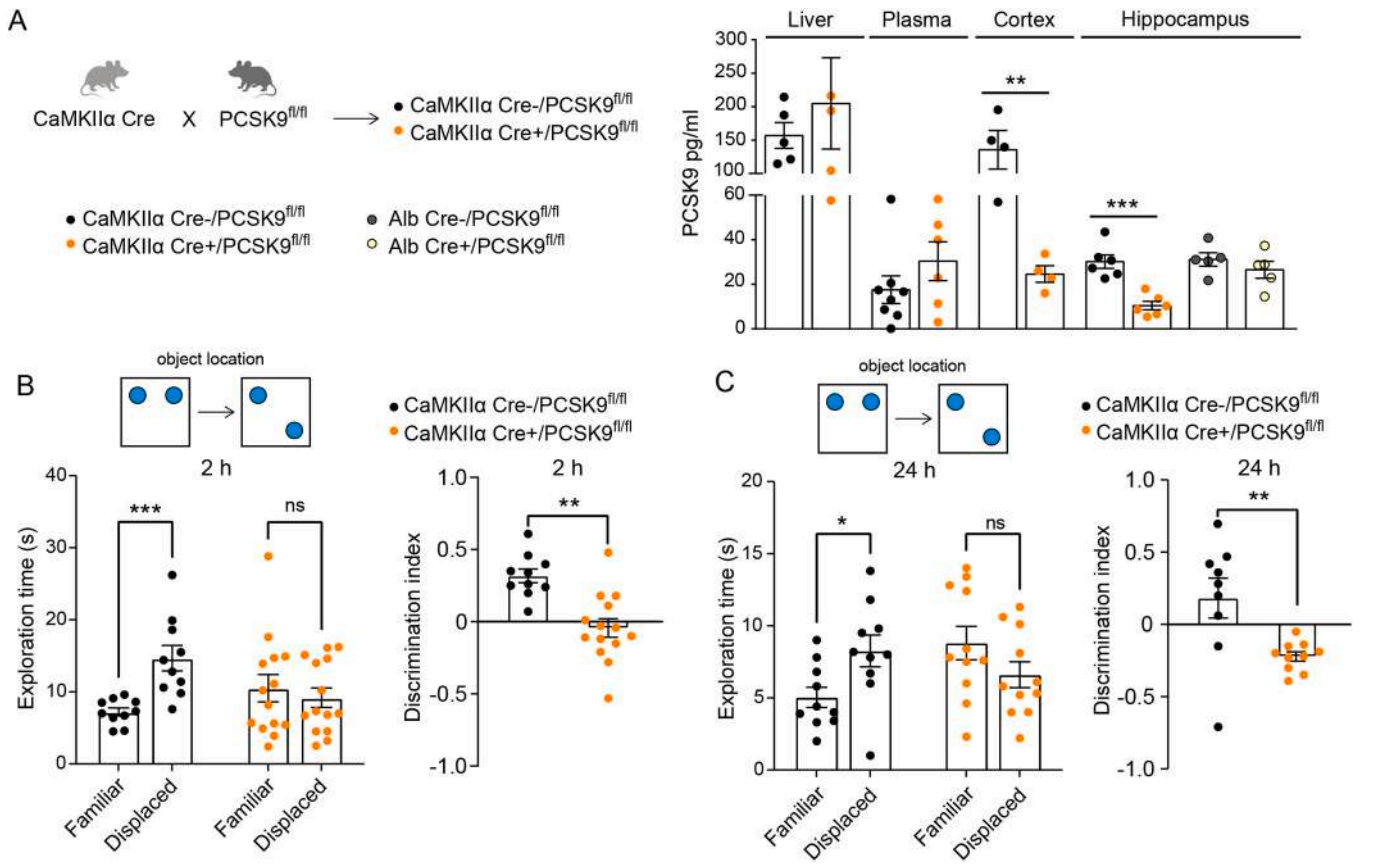

Fig. 2. Cognitive impairment in CaMKIIα Cre^{+}/PCSK9$^{fl/fl}$ mice. A. PCSK9$^{fl/fl}$ mice were crossed with CaMKIIα-Cre to generate mice selectively lacking PCSK9 production in Ca^{2+}- CaMKIIα-expressing neurons. Right, results of ELISA measuring PCSK9 concentration in liver, plasma, cortex, and hippocampus of CaMKIIα Cre^{+}/PCSK9$^{fl/fl}$ and control CaMKIIα Cre^{-}/PCSK9$^{fl/fl}$ mice. Significant reduction in PCSK9 levels was detected in the cortex and hippocampus of CaMKIIα Cre^{+}/PCSK9$^{fl/fl}$ compared to CaMKIIα Cre^{-}/PCSK9$^{fl/fl}$ mice (cortex, n = 4 mice, two-tailed unpaired *t*-test, t = 3.810, df = 6, ** P = 0.0089; hippocampus, n = 6 mice, two-tailed unpaired *t*-test, t = 5.482, df = 10, *** P = 0.0003). PCSK9 concentrations were not affected in the hippocampus of Alb Cre^{+}/PCSK9$^{fl/fl}$ compared to Alb Cre^{-}/PCSK9$^{fl/fl}$ mice. B. Schematic of the novel object recognition test. Left, exploration time (in seconds) of familiar and novel objects of CaMKIIα Cre^{+}/PCSK9$^{fl/fl}$ (n = 14) control (CaMKIIα Cre^{-}/PCSK9$^{fl/fl}$, n = 10) mice in the object location recognition task 2 h after sample phase (two-way RM ANOVA, objects x genotype, $F_{(1,22)}$ = 19.32, P = 0.0002). Right, discrimination index displayed by CaMKIIα Cre^{+}/PCSK9$^{fl/fl}$ and control CaMKIIα Cre^{-}/PCSK9$^{fl/fl}$ mice in the object location recognition task 2 h after sample phase (two-tailed unpaired *t*-test, t = 4.20, df = 22, P = 0.0004). C. Schematic of the novel object recognition test. Left, exploration time (in seconds) of familiar and displaced objects of CaMKIIα Cre^{+}/PCSK9$^{fl/fl}$ (n = 10) and control (CaMKIIα Cre^{-}/PCSK9$^{fl/fl}$, n = 11) mice in the object location recognition task 24 h following the sample phase (two-way RM ANOVA, objects x genotype, $F_{(1,19)}$ = 9.07, P = 0.0072). Right, discrimination index displayed by CaMKIIα Cre^{+}/PCSK9$^{fl/fl}$ and control CaMKIIα Cre^{-}/PCSK9$^{fl/fl}$ mice in the object location recognition task 24 h following the sample phase (two-tailed unpaired *t*-test, t = 2.98, df = 17, P = 0.0083).

the AMPAR subunit GluA1, nor its phosphorylation of Ser845, which is associated with increased AMPAR trafficking to the postsynaptic membrane, were detected in CaMKIIα Cre^{+}/PCSK9$^{fl/fl}$ mice (Suppl. Fig. 2B-C).

Next, we measured the total and synaptic levels of PCSK9 brain targets. As shown in Fig. 4C, no changes in the levels of LDLR, LRP1, VLDLR, or ApoER2 were found in the hippocampal homogenates of CaMKIIα Cre^{+}/PCSK9$^{fl/fl}$ mice compared to controls. On the other hand, analysis of the postsynaptic compartment showed that ApoER2 synaptic localization was specifically increased in CaMKIIα Cre^{+}/PCSK9$^{fl/fl}$ mice compared to controls; there were no changes in the synaptic abundance of LDLR, LRP1, or VLDLR (Fig. 4D).

ApoER2 is a Reelin receptor that can activate a signaling cascade through Dab1 and SFK pathways to phosphorylate GluN2B in tyrosine (Tyr) residues [46]. Considering the increase in GluN2B synaptic abundance in CaMKIIα Cre^{+}/PCSK9$^{fl/fl}$ mice (Fig. 4B), we tested whether this change in GluN2B localization could be related to increased Tyr phosphorylation. Tyr phosphorylation of immunoprecipitated GluN2B was detected by immunoblotting using a pY20 antibody. No changes in Tyr phosphorylation of GluN2B were detected in CaMKIIα Cre^{+}/PCSK9$^{fl/fl}$ compared to control mice (Suppl. Fig. 2D). We also assessed the phosphorylation levels at Tyr1472 of GluN2B; this stabilizes synaptic NMDARs by preventing the interaction of the clathrin adaptor protein with the YEKL motif on GluN2B [47]. Western blot analysis of the postsynaptic fraction showed that GluN2B phosphorylation at Tyr1472 is not altered in CaMKIIα Cre^{+}/PCSK9$^{fl/fl}$ mice compared to controls (Suppl. Fig. 2E), suggesting that other molecular modifications are responsible for the changes in GluN2B synaptic localization.

3.4. PCSK9 plays a critical role in controlling synaptic membrane insertion of ApoER2 and lipid droplet trafficking

To gain insights into PCSK9-dependent regulation of ApoER2 in neurons, we took advantage of an in vitro model, primary hippocampal cultures.

First, we verified the synaptic localization of LDLR, LRP1, and ApoER2 in our cellular system using confocal imaging. As shown in Supplementary Fig. 3A–C, all analyzed receptors were present in dendritic spines close to the area enriched with the postsynaptic marker PSD-95.

As PCSK9 targets are synaptic proteins, we tested whether synaptic activity could modulate the expression of PCSK9 targets in hippocampal

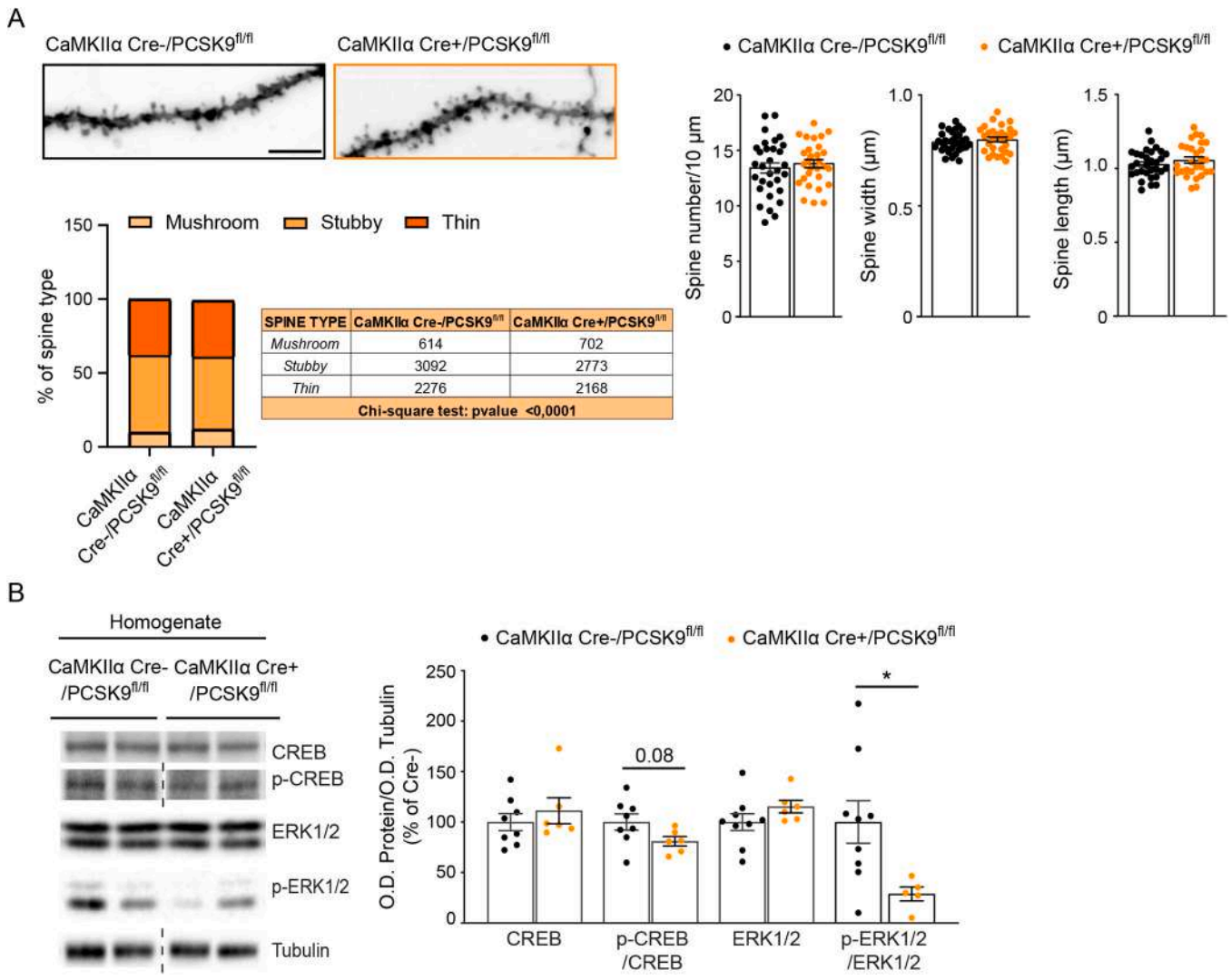

Fig. 3. Alterations in dendritic spine morphology and synaptic plasticity-related signaling in the hippocampus of CaMKIIα Cre^{+}/PCSK9$^{fl/fl}$ mice. A. Left, representative confocal images of hippocampal dendritic spines of CaMKIIα Cre^{-}/PCSK9$^{fl/fl}$ and CaMKIIα Cre^{+}/PCSK9$^{fl/fl}$ mice. Scale bar: 5 µm. Right, quantification of spine density, spine width and length showed no significant changes in these parameters (n = 31 neurons from four CaMKIIα Cre^{-}/PCSK9$^{fl/fl}$ mice, n = 29 neurons from four CaMKIIα Cre^{+}/PCSK9$^{fl/fl}$ mice). Below, the joint distribution of dendritic spine type and genetic modification is represented in the table together with the P value of the Chi-squared test of independence. B. Representative western blot (WB) showing the expression of CREB, p-CREB, ERK1/2, p-ERK1/2, and tubulin in hippocampal homogenate samples of CaMKIIα Cre^{+}/PCSK9$^{fl/fl}$ compared to CaMKIIα Cre^{-}/PCSK9$^{fl/fl}$ animals. Quantification of optical density (OD) and normalization to loading control OD (tubulin) shows that p-ERK1/2, but not ERK total levels, is reduced in CaMKIIα Cre^{+}/PCSK9$^{fl/fl}$ mice (p-CREB /CREB: CaMKIIα Cre^{-}/PCSK9$^{fl/fl}$ n = 8 mice and CaMKIIα Cre^{+}/PCSK9$^{fl/fl}$ n = 6 mice, two-tailed unpaired *t*-test, t = 1.878, df = 12, P = 0.08; p-ERK1/2/ERK1/2: CaMKIIα Cre^{-}/PCSK9$^{fl/fl}$ n = 9 mice and CaMKIIα Cre^{+}/PCSK9$^{fl/fl}$ n = 5 mice, two-tailed unpaired *t*-test, t = 2.434, df = 12, * P = 0.03).

neurons. RT-qPCR analysis of PCSK9 targets revealed a reduction in *ApoER2* mRNA levels after 30 min of synaptic stimulation, while *LDLR* and *Lrp1* expression was not affected by synaptic activation (Suppl. Fig. 3D). As control of the treatment, we found that synaptic stimulation increased the transcription of the immediate early gene *Arc* in primary neuronal cultures (Suppl. Fig. 3E).

To test the effects of reduced PCSK9 activity in hippocampal cultures, we used a small hairpin RNA (shRNA) to downregulate PCSK9 expression [42]. We first verified that the shRNA was able to reduce the levels of co-transfected PCSK9-FLAG in heterologous cells (shPCSK9, Suppl. Fig. 3F).

We transfected primary hippocampal neurons with a vector expressing either shPCSK9 or a scramble sequence (SCR), and the fluorescent mCherry protein expressed under the control of CaMKIIα, to allow visualization of the neuronal structure.

We observed a significant increase in the degree of co-localization between ApoER2 and the postsynaptic marker PSD-95 in neurons transfected with shPCSK9, compared with those transfected with the scramble control sequence (Fig. 5A). This indicates enrichment of ApoER2 at synapses, in line with the data obtained in CaMKIIα Cre^{+}/PCSK9$^{fl/fl}$ mice (Fig. 4D).

However, the relative expression of ApoER2 at the membrane surface was significantly reduced in primary hippocampal neurons expressing shPCSK9 compared with control cells (Fig. 5B). Similar results were obtained by quantifying the ApoER2 surface expression within PSD-95 postsynaptic clusters (Fig. 5B). These data show that the ApoER2 increase in PSD-95-positive dendritic spines does not correspond to augmented synaptic membrane insertion of ApoER2.

Extensive studies have established the role of ApoE in mediating inter-cellular cholesterol transport from non-neuronal to neuronal cells [48,49]. In neurons, internalization of cholesterol from ApoE-containing lipoproteins is mediated by the LDLR family [11]. We therefore tested whether the reduction in ApoER2 membrane insertion in shPCSK9-transfected cells could affect lipid droplet transfer. Neuronal

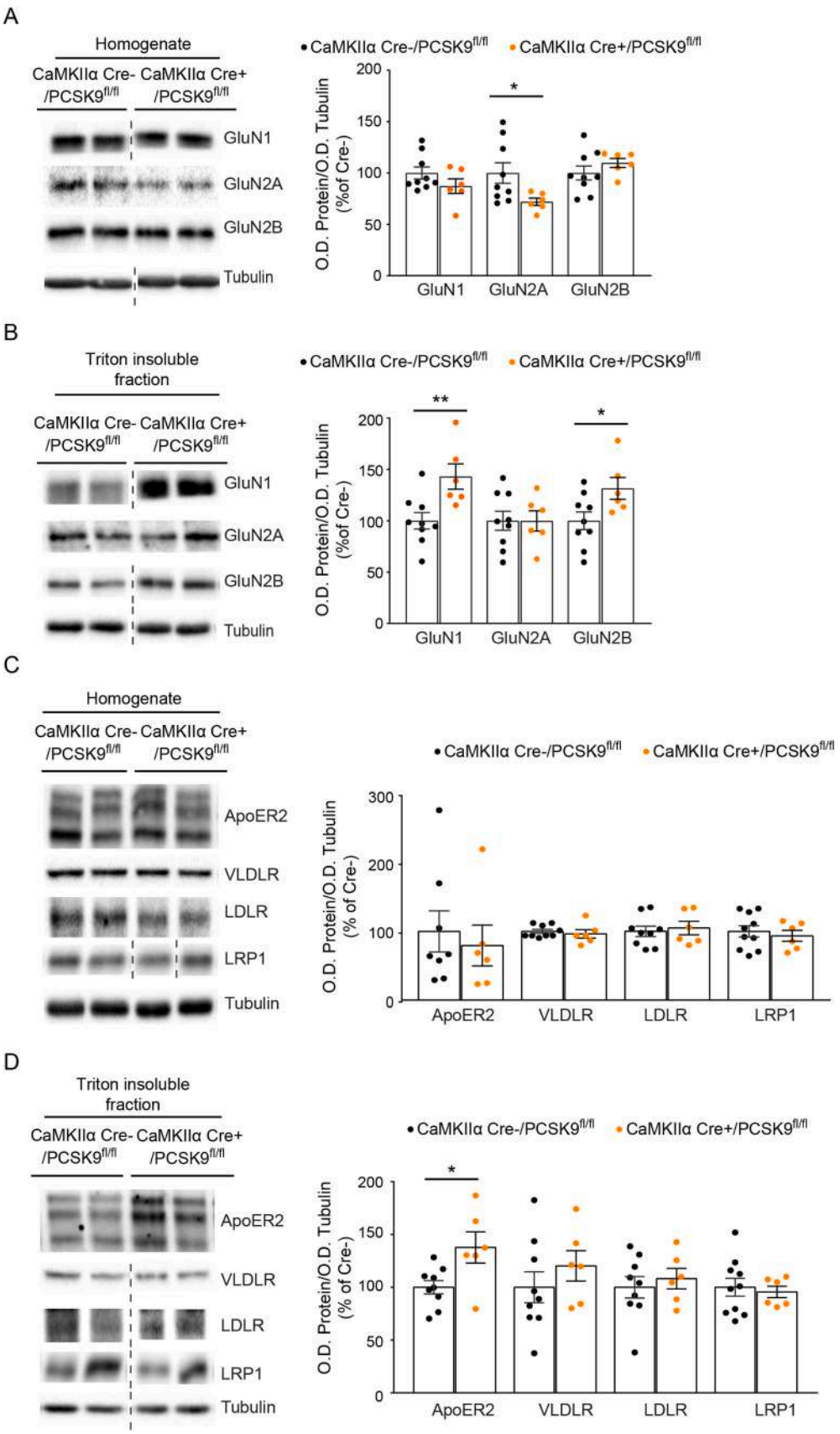

(caption on next page)

Fig. 4. NMDAR and ApoER2 are changed in hippocampal synapses of CaMKIIα Cre^{+}/PCSK9$^{fl/fl}$ mice. A. Representative WB showing the expression of GluN1, GluN2A, GluN2B and tubulin, as the loading control, in hippocampal homogenate samples of CaMKIIα Cre^{+}/PCSK9$^{fl/fl}$ and CaMKIIα Cre^{-}/PCSK9$^{fl/fl}$ animals. Statistical analysis shows that GluN2A total levels are reduced in CaMKIIα Cre^{+}/PCSK9$^{fl/fl}$ mice (n = 6) compared to CaMKIIα Cre^{-}/PCSK9$^{fl/fl}$ animals (n = 9) (GluN2A: two-tailed unpaired *t*-test, t = 2.205, df = 13, * P = 0.046). B. Representative WB showing the levels of GluN1, GluN2A, GluN2B, and tubulin in the postsynaptic fraction (TIF, Triton-Insoluble Fraction) of CaMKIIα Cre^{+}/PCSK9$^{fl/fl}$ and CaMKIIα Cre^{-}/PCSK9$^{fl/fl}$ animals. Statistical analysis shows that GluN1 and GluN2B synaptic levels are increased in CaMKIIα Cre^{+}/PCSK9$^{fl/fl}$ mice (n = 6) compared to CaMKIIα Cre^{-}/PCSK9$^{fl/fl}$ animals (n = 9) (GluN1: two-tailed unpaired *t*-test, t = 3.077, df = 13, ** P = 0.0088; GluN2B: two-tailed unpaired *t*-test, t = 2.311, df = 13, * P = 0.038). C. Representative WB of ApoER2, VLDLR, LDLR, LRP1, and tubulin in hippocampal homogenate samples of CaMKIIα Cre^{+}/PCSK9$^{fl/fl}$ and CaMKIIα Cre^{-}/PCSK9$^{fl/fl}$ mice. OD quantification and normalization on loading control OD (tubulin) reveals no differences in expression in CaMKIIα Cre^{+}/PCSK9$^{fl/fl}$ (n = 6) compared to CaMKIIα Cre^{-}/PCSK9$^{fl/fl}$ (n = 9). D. Representative WB of the postsynaptic levels of ApoER2, VLDLR, LDLR, LRP1, and tubulin in TIF purified from CaMKIIα Cre^{+}/PCSK9$^{fl/fl}$ and CaMKIIα Cre^{-}/PCSK9$^{fl/fl}$ hippocampi. ApoER2 levels are increased in CaMKIIα Cre^{+}/PCSK9$^{fl/fl}$ mice (n = 6) compared to CaMKIIα Cre^{-}/PCSK9$^{fl/fl}$ animals (n = 9) (ApoER2: two-tailed unpaired *t*-test, t = 2.672, df = 13, * P = 0.019).

cultures transfected with either shPCSK9 or the scramble control sequence, with GFP as a reporter gene, were stained with Nile Red to selectively label lipid droplets. Quantitative analysis showed a significant increase in lipid droplets in shPCSK9-transfected neurons compared with SCR-expressing cells, indicating that PCSK9 downregulation affects lipid droplet transport (Fig. 5C). This hypothesis is supported by the analysis of cholesterol in the hippocampus of both PCSK9$^{-/-}$ and CaMKIIα Cre^{+}/PCSK9$^{fl/fl}$ mice and the correspondent control animals (Suppl. Fig. 3G). The cholesterol levels are increased in both animal models, suggesting that the lack of PCSK9 significantly impairs cholesterol metabolism.

3.5. PCSK9 is crucial for maintaining synaptic function in hippocampal neurons

Considering the relevance of cholesterol metabolism and lipid droplet trafficking to synaptogenesis [49] and synapse maintenance [50], we assessed the effect of PCSK9 downregulation on synaptic function.

First, we analyzed spine and neuronal structure. Spine analysis revealed a significant reduction in spine density in shPCSK9-transfected neurons. The evaluation of spine shape revealed a significant increase in spine head width, without changes in spine length (Fig. 6A). The quantification of different spine categories showed that different spine populations were associated with PCSK9-down-regulation. Furthermore, we measured a significant increase in the width of mushroom and stubby spines in shPCSK9-transfected neurons (Fig. 6A). Next, we analyzed neuronal morphology by Sholl analysis, a common method used to quantify neuronal complexity, in neurons expressing either shPCSK9 or the control sequence. PCSK9 downregulation did not affect neuronal arborization and dendritic length (Suppl. Fig. 3H). These data suggest that the downregulation of PCSK9 specifically affects spine morphology and not neuronal architecture.

We subsequently asked whether decreased PCSK9 expression could influence synaptic activity. Firstly, we measured the phosphorylation of the transcription factor CREB at Ser133. This is a key element coupling synaptic activation to the transcription of genes and is required for long-term synaptic plasticity events and memory formation [51]. As shown in Fig. 6B, the downregulation of PCSK9 expression significantly reduced CREB phosphorylation in the nucleus, rendering CREB transcriptionally inactive and thus impairing synaptic plasticity.

Secondly, we recorded miniature excitatory postsynaptic currents (mEPSCs) in shPCSK9-transfected neurons and their controls. Analysis revealed normal mEPSC frequency but significant increases in the amplitude of AMPAR-mediated currents (Fig. 6C). These results suggest a direct contribution of PCSK9 to synaptic AMPAR accumulation and leads us to hypothesize that the increased head width found in mushroom and stubby spines in shPCSK9 cultures (Fig. 6A) may allow the insertion of more functional AMPARs.

Considering these results, we investigated the synaptic localization of the AMPAR subunit GluA1. In line with the electrophysiological results, confocal imaging showed that PCSK9 downregulation significantly increased the proportion of GluA1-stained pixels colocalizing with the postsynaptic marker PSD-95, when compared to control neurons (Fig. 7A). Measuring the colocalization of NMDAR subunits with PSD-95, no change was observed to the obligatory subunit GluN1 in shPCSK9-transfected neurons. This suggests that downregulation of PCSK9 does not affect synaptic NMDAR levels (Fig. 7B). The colocalization of GluN2B and PSD-95 was however significantly reduced, suggesting an effect on NMDAR subunit composition (Fig. 7C); no changes in GluN2A synaptic localization were detected (Fig. 7D). Overall, these data highlight PCSK9 as a protein relevant for synaptic structure and function.

4. Discussion

PCSK9 inhibitors are largely used to decrease plasma LDL-C levels and reduce cardiovascular risk. Yet, PCSK9 was initially discovered as a gene upregulated after apoptosis induced by serum deprivation in primary cerebellar neurons [25]. Despite its initial identification in the brain, the molecular pathways involved in neuronal PCSK9 function remain largely elusive and a matter of considerable debate. In this study, we demonstrated that the deletion of neuronal PCSK9 affects the structure and molecular composition of hippocampal dendritic spines, leading to impaired cognitive function. Notably, among the various targets of PCSK9, we identified ApoER2 as the primary mediator of PCSK9-dependent effects on synaptic function.

Previous studies have investigated the role of PCSK9 during brain development and in different cellular models of neurogenesis and neuronal differentiation [25,30,52,53]. Our study aimed to investigate the contribution of PCSK9 to neuronal function during adulthood. To achieve this goal, we used *in vivo* and *in vitro* models to assess the effect of PCSK9 deletion on neuronal cells.

First, we evaluated the cognitive performance of PCSK9$^{-/-}$ mice. We found that systemic deletion of PCSK9 leads to recognition memory deficits, particularly when mice are required to recall spatial information. These deficits were not explained by reduced interest in exploration or locomotor impairments. A recent study showed that PCSK9$^{-/-}$ mice have intact spatial navigation and learning capabilities [53]. However, in our setting, PCSK9$^{-/-}$ mice also showed recognition impairment during memory recall regarding familiarity of a previous encounter. Thus, our results suggest that PCSK9 is more involved in memory formation or consolidation rather than the processing of spatial information. Consistently, memory defects in PCSK9$^{-/-}$ mice were accompanied by alterations of spine morphology in the hippocampus, a critical brain area for spatial memory. Dendritic spines are the neuronal locus of plasticity as modification of synaptic strength can be transformed into long-lasting morphological changes [54]. These changes are reflected in cognitive performance. In PCSK9$^{-/-}$ mice, we observed a decrease in the amount of mature mushroom-shaped spines in the hippocampus, suggesting that the lack of PCSK9 may affect synaptic plasticity-related phenomena. The significant impairments observed in the object location task and the morphological changes in hippocampal spines suggested a critical role for PCSK9 in hippocampal function. Therefore, we focused this study on the hippocampus, although exploring the role of PCSK9 in cortical neurons would be an intriguing

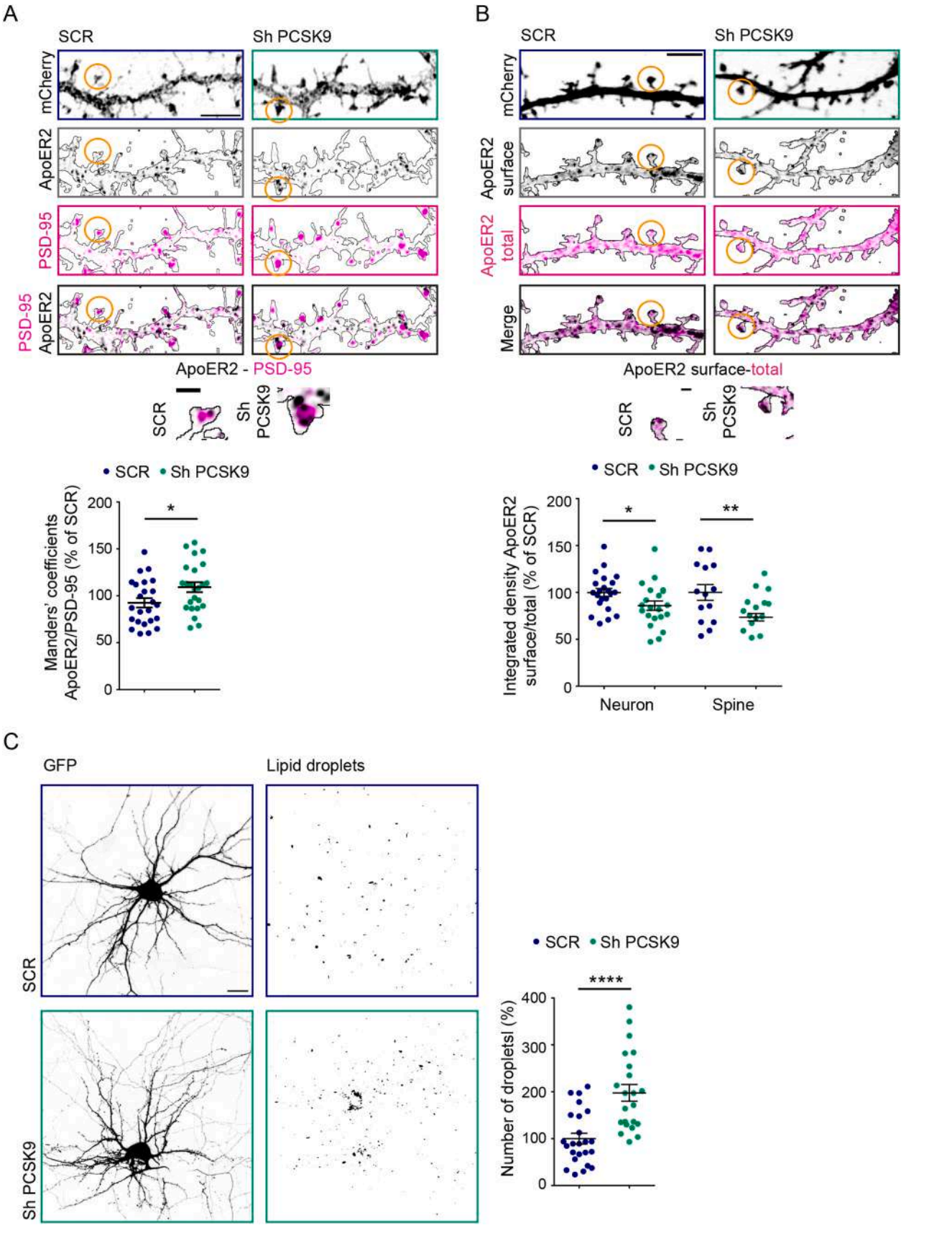

(caption on next page)

Fig. 5. PCSK9 downregulation affects ApoER2 membrane levels and lipid droplets. A. Representative confocal images of mCherry (neuronal filler), ApoER2 (black), and PSD-95 (magenta) staining in primary hippocampal neurons transfected with PCSK9-shRNA (shPCSK9) or scramble sequence (SCR) plasmids expressing mCherry; scale bar = 5 μm. Lower images, insets showing dendritic spines at higher magnification; scale bar = 1 μm. The downregulation of PCSK9 increases ApoER2 colocalization with PSD-95 (n = 24 neurons, two-tailed unpaired *t*-test, t = 2.294, df = 46, * P = 0.026). B. Representative confocal images of mCherry, ApoER2 surface staining (black), and ApoER2 total staining (magenta) of primary hippocampal neurons transfected with shPCSK9 or SCR plasmids expressing mCherry; scale bar = 5 μm. Lower images, insets showing dendritic spines at higher magnification; scale bar = 1 μm. The downregulation of PCSK9 reduces ApoER2 membrane levels both at neuronal levels and in spines (neuron, n = 22–21, two-tailed unpaired *t*-test, t = 2.147, df = 41, * P = 0.038; spine, n = 14–15, two-tailed unpaired *t*-test, t = 2.881, df = 27, * P = 0.0077). C. Representative confocal images of lipid droplets and GFP staining in primary hippocampal neurons transfected with shPCSK9 or SCR plasmids expressing GFP, scale bar = 20 μm; PCSK9 silencing significantly increases lipid droplets (n = 24 – 22 neurons, Mann Whitney test, **** P < 0.0001).

direction for future research.

PCSK9$^{-/-}$ mice could not be the ideal model for investigating the role of PCSK9 in neurons due to the many pleiotropic effects of PCSK9 in different organs beyond the liver [55] giving rise to a complex phenotype. This complexity makes it difficult to isolate a brain-specific effect. Additionally, the ablation of PCSK9 during embryonic development may drive compensation mechanisms masking PCSK9 function in the brain.

Therefore, to address the impact of the postnatal deletion of PCSK9 in excitatory neurons, we generated neuron-selective PCSK9-deficient mice. Given that the neuronal ablation of PCSK9 does not affect the circulating levels of either the protein, total cholesterol or triglycerides, CaMKIIα Cre^{+}/PCSK9$^{fl/fl}$ mice provide a reliable model for investigating the effects of neuronal PCSK9 inactivation.

Behavioral results revealed the alteration of both short- and long-term spatial recognition memory in CaMKIIα Cre^{+}/PCSK9$^{fl/fl}$ mice, similar to the effects observed in the full-body knock-out mice. At the cellular level, hippocampal neurons of CaMKIIα Cre^{+}/PCSK9$^{fl/fl}$ mice showed a modest decrease in the percentage of stubby spines and a moderate increase in mature mushroom spines. These results seem to be in contrast with the impairment of cognitive function demonstrated in the behavioral tests. However, biochemical analysis revealed significant changes in the molecular composition of the postsynaptic compartment and the shut-off of signaling pathways critical for synaptic plasticity. In particular, we detected a significant modification of different NMDAR subunits, namely a reduction in total GluN2A levels, and enrichment of GluN2B-containing NMDARs in CaMKIIα Cre^{+}/PCSK9$^{fl/fl}$ mice synapses. In addition, we found a significant shut-off of signaling pathways mediated by ERK, supporting the hypothesis that inactivation of neuronal PCSK9 can affect synaptic plasticity. In the mature hippocampus, GluN2A and GluN2B are the predominant GluN2 subunits. In mature neurons, most GluN2A-containing NMDARs are synaptically retained, while GluN2B-containing NMDARs are highly mobile and localized at extra-synaptic sites [56,57]. Considering that GluN2A and GluN2B have antagonistic actions on ERK activation, the negative regulation of ERK in CaMKIIα Cre^{+}/PCSK9$^{fl/fl}$ mice hippocampi could depend on the composition of NMDARs. In particular, the synaptic Ras GTPase activating protein (GAP) SynGAP is selectively associated with GluN2B-NMDARs in the brain and is required for inhibition of NMDAR-dependent ERK activation [58].

The generation of this transgenic mouse line has also provided insights into the primary target of PCSK9 in neuronal functionality. The abundance of ApoER2 is significantly increased in CaMKIIα Cre^{+}/PCSK9$^{fl/fl}$ mice synapses, while total protein levels remain unaffected. Interestingly, the total and synaptic levels of LDLR, LRP1, and VLDLR in these mice are meanwhile unaltered. Previous studies have reported contrasting results on whether PCSK9 targets LDLR, VLDLR, or ApoER2 for degradation depending on the model or the cell line. *In vitro*, PCSK9 has been shown to reduce LDLR abundance in neurons in the early stages of differentiation [53]. *In vivo*, LDLR protein levels are significantly higher in PCSK9$^{-/-}$ mouse embryos, but they are not affected in adult animals [27]. Similarly, modulation of PCSK9 expression did not change LDLR, VLDLR, or ApoER2 expression levels in the hippocampus or cerebral cortex of adult mice [29].

Our results demonstrate, for the first time, that PCSK9 controls the synaptic localization of ApoER2 in hippocampal neurons. Furthermore, taking advantage of an *in vitro* system, we found that downregulation of PCSK9 increases synaptic localization of ApoER2, as indicated in our mouse model. However, the enrichment of ApoER2 at the postsynaptic site is accompanied by a decrease in the membrane level of the receptor, indicating increased endocytosis in the absence of PCSK9. ApoER2 is a postsynaptic protein involved in multiple cellular signaling cascades, synaptic plasticity phenomena, and learning and memory processes [59,60]. Indeed, we found that synaptic stimulation reduces ApoER2 gene expression without affecting the mRNA levels of other synaptic members of the LDLR family, such as LDLR and LRP1.

The reduction of ApoER2 membrane availability could be implicated in the synaptic changes observed in shPCSK9-transfected neurons. It has been shown that ApoER2 controls synapse formation as its overexpression increases spine density and decreases GluA1 surface levels in primary neurons [61]. ApoER2 may be coupled to synaptic function through various mechanisms since it works as a mediator of Reelin signaling and contributes to cholesterol homeostasis through its binding to lipidated ApoE particles secreted by astrocytes [10]. The definitive mechanism by which ApoER2 acts remains unknown. Here, we hypothesize that the lack of PCSK9 and dysregulation of ApoER2 membrane insertion can affect lipid transport, as suggested by the increase in lipid droplets in neurons transfected with shPCSK9. Consistently, we found an increase in cholesterol levels in CaMKIIα Cre^{+}/PCSK9$^{fl/fl}$ mice hippocampi, thus highlighting the crucial role of neuronal PCSK9 in the control of cholesterol in the brain. In neurons, membrane lipid rafts have been detected at synapses, where they are thought to contribute to postsynaptic function by altering the physical properties of the membrane bilayer. Consequently, they can influence receptor dynamics at postsynapses [1]. For instance, depletion of cholesterol/sphingolipid leads to instability of surface AMPARs and loss of dendritic spines, while the remaining spines in raft-depleted neurons become greatly enlarged [50]. A similar phenotype is detected in shPCSK9 transfected neurons, which show reduced spine density and expansion of head size, together with an increase in GluA1 synaptic localization and mEPSC amplitude. These synaptic modifications mimicking LTP-like changes may occlude synaptic plasticity. Similarly, in CaMKIIα Cre^{+}/PCSK9$^{fl/fl}$ mice we detected a slight increase in the number of mature mushroom spines, suggesting that occlusion of synaptic plasticity mechanisms can also occur *in vivo*. Even though the molecular characterization of the postsynaptic compartment of CaMKIIα Cre^{+}/PCSK9$^{fl/fl}$ mice and shPCSK9 transfected neurons provided differing results, in both models we found a decrease in CREB phosphorylation, strengthening the hypothesis that lack of neuronal PCSK9 significantly impairs synaptic plasticity. We hypothesize that *in vivo* there may be mechanisms to compensate for the inactivation of PCSK9.

In conclusion, taking advantage of different models, we have demonstrated a key role for neuronal PCSK9 in synaptic function and cognitive behavior during adulthood. PCSK9 acts at the synaptic level controlling the availability of ApoER2, a key protein positioned at the crossroads of multiple pathways implicated in synaptic plasticity. Our results provide new insights into the complex biology of PCSK9, which are essential for assessing the potential side effects of PCSK9-targeting therapies and for advancing the development of novel therapeutic strategies that leverage PCSK9 as a target for neurological diseases.

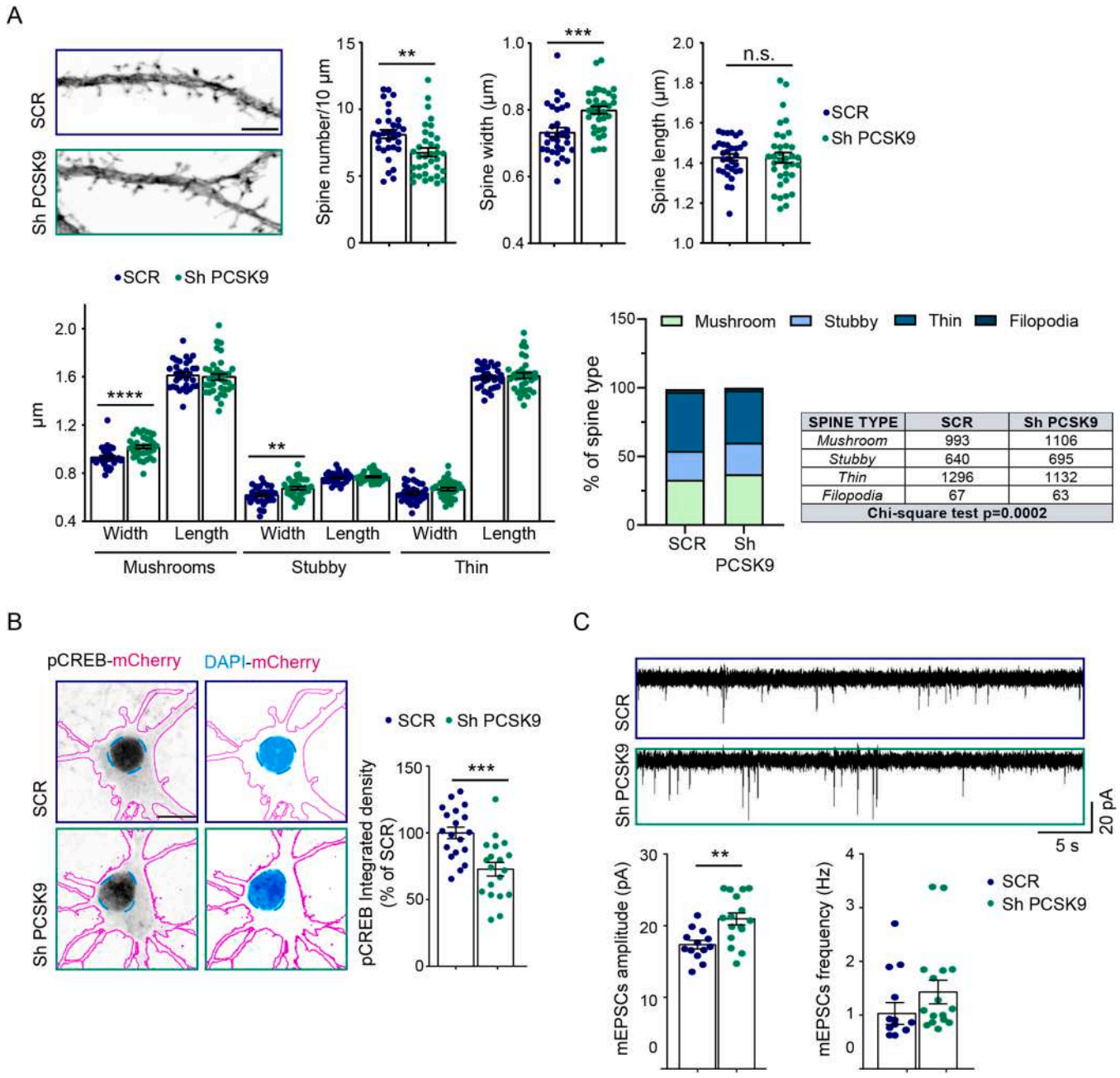

Fig. 6. PCSK9 silencing impairs spine morphology and synaptic transmission. A. Representative confocal images of mCherry staining of primary hippocampal neurons transfected with shPCSK9 or scramble sequence (SCR) plasmids expressing mCherry as neuronal filler; scale bar = 5 µm. PCSK9 down-regulation decreases spine density, increases spine head width, in particular in mushroom and stubby spines (n = 32–35 neurons; spine density, Mann Whitney test, ** P = 0.0019; spine width, two-tailed unpaired *t*-test, t = 3.784, df = 65, *** P = 0.0003; mushroom spine width, Mann Whitney test, **** P < 0.0001; stubby spine width, two-tailed unpaired *t*-test, t = 3.175, df = 65, ** P = 0.0023). The joint distribution of dendritic spine type and genetic modification is represented in the table together with the P value of the Chi-squared test of independence. B. Representative confocal images of p-CREB (black) staining of primary hippocampal neurons transfected with shPCSK9 or SCR plasmids expressing mCherry as neuronal filler; nuclei were detected with DAPI (blue). Scale bar = 5 µm. The downregulation of PCSK9 significantly reduces p-CREB nuclear levels (n = 19 neurons, two-tailed unpaired *t*-test, t = 4.035, df = 36, *** P = 0.0003). C. Representative traces of excitatory postsynaptic current in miniature (mEPSCs) recorded in shPCSK9 and SCR control neurons followed by quantitative analysis. Histograms represent the mean ± SEM of the mEPSCs amplitude and frequency expressed respectively in pA and Hz; PCSK9 silencing affects mEPSCs amplitude but not the frequency (mEPSCs amplitude, two-tailed unpaired *t*-test, t = 3.318, df = 27, ** P = 0.0026).

Funding sources

This project has received funding from Italian Ministry of Research and University (MUR) (PRIN 20202THZAW, PRIN2022 PNRR P2022TKN8C, FIS00000560 - Stone, PNRR, Missione 4 – Componente 2–Investimento 1.3, finanziato dall'Unione europea – NextGenerationEU "Fascination" to MDL, PRIN202039WMFP, PRIN2022 PNRR P2022R2E8N to EM, PRIN 2022 7KTSAT to GDN, PRIN 2022 2022NBKCWP to FB, PRIN 2022 20229XWM5L to FA), from the Giovanni Armenise Harvard Foundation and AIRALZH ONLUS (2023 Armenise Harvard-AIRALZH Mid-Career Award in Neurodegenerative Diseases - AHA MCA- to EM), from the Italian Ministry of Enterprises and Made in Italy (PNRR - Next generation EU funding, "SEED for Innovation Patent 2.0" program, project TT_MIN23_SEED4IP2.0_07 to EM), from

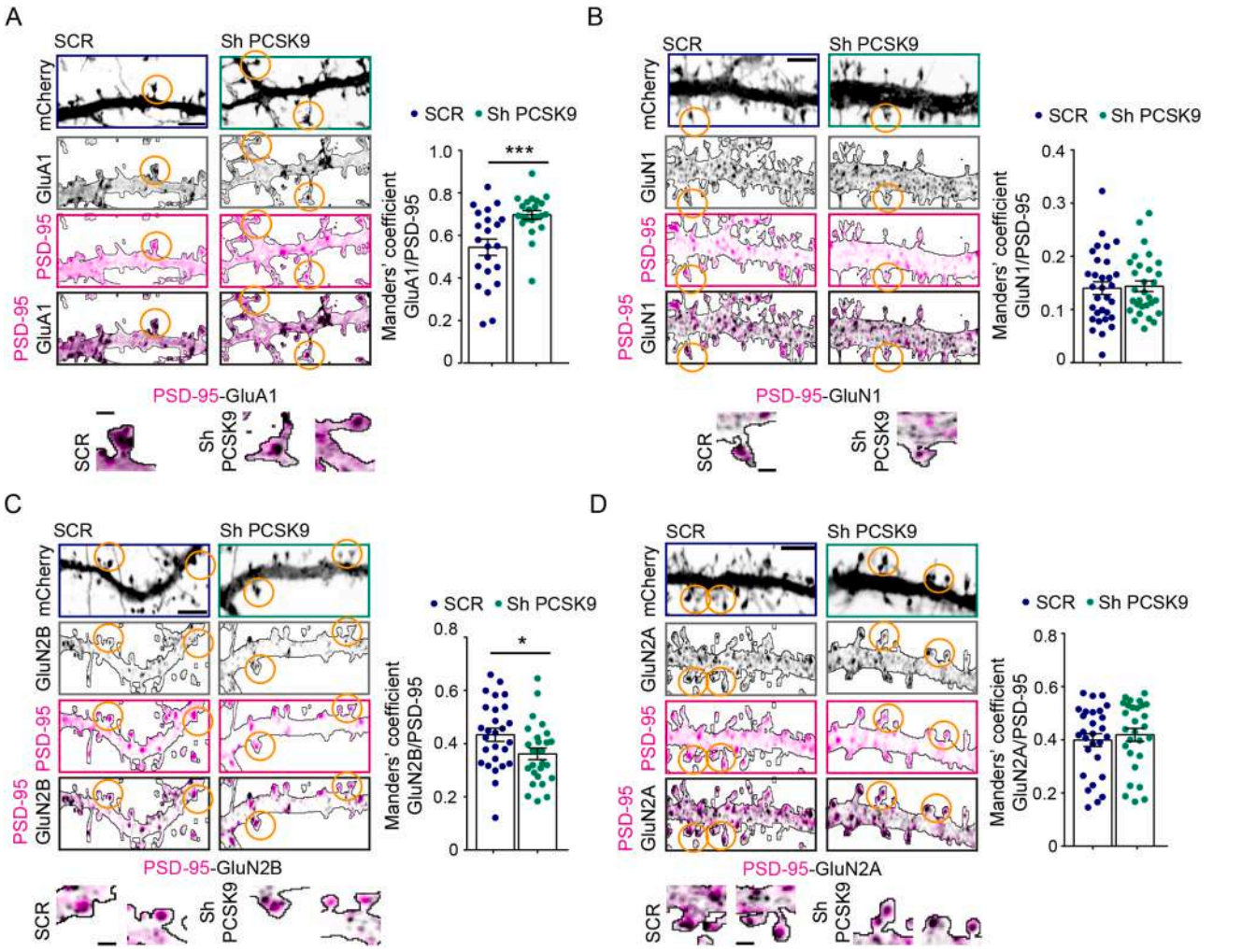

Fig. 7. PCSK9 affects the synaptic localization of AMPAR and NMDAR. A Representative confocal images of dendrites of hippocampal neurons transfected with PCSK9-shRNA (shPCSK9) or scramble sequence (SCR) plasmids, expressing mCherry as neuronal filler, and stained with PSD-95 (magenta) and GluA1 (A), GluN1 (B), GluN2B (C) and GluN2A (D) (black). Scale bars = 5 μm. Lower images, insets showing dendritic spines at higher magnification; scale bar = 1 μm. Bar graph represents the percentage of co-localization between GluA1 (A), GluN1 (B), GluN2B (C), and GluN2A (D) and PSD-95. PCSK9 silencing affects GluA1 and GluN2 synaptic localization (GluA1: n = 22–21 neurons, two-tailed unpaired *t*-test, t = 4.010, df = 41, *** P = 0.0003; GluN2B: n = 27 neurons, two-tailed unpaired *t*-test, t = 2.202, df = 52, * P = 0.03).

the European Atherosclerosis Society (EAS) Research Grant 2023 (to LDD), from Ricerca Finalizzata, Ministry of Health (RF-2019–12370896 to GDN), Nanokos (European Commission Ref EUROPEAID/173691/DD/ACT/XK to GDN), PNRR Missione 4 (Progetto CN3 - National Center for Gene Therapy and Drugs based on RNA Technology to GDN), PNRR Missione 4 (Progetto MUSA- Multilayered Urban Sustainability Action to GDN), PNRR Missione 6 (PNRR-MAD-2022–12375913 to GDN), CARDINNOV, Ministry of Research and University under the umbrella of the Partnership Fostering a European Research Area for Health (ERA4-Health) (GA N° 101095426 of the EU Horizon Europe Research and Innovation Programme to GDN) from Fondazione Cariplo (1560–2019 to FB), from Telethon Seed Grant Spring 2022 RETT (N. 4196 to FA), from Associazione Nazionale Atassia Telangiectasia (ANAT2022 to FA) and from the Matteo Caleo Foundation, [www.matteocaleofoundation.org (accessed on 19 July 2023) to FA], from Piano di Sostegno alla Ricerca (PSR), Università degli Studi di Milano (PSR2022_DIP_022_AZIONE_A_SPELU to SP, PSR2022_DIP_022_AZIONE_A_FBONA to FB, PSR 2021 and 2022 to DS). This work was partially supported by MUR, code MUR 2022ZW3M8H (Bando PRIN 2022 - DD 104 del 02/02/2022) - CUP "C53D23006260006 to NF.

This work was also supported by MUR Progetto Eccellenza (2022–2027) to the Dipartimento di Scienze Farmacologiche e Biomolecolari "Rodolfo Paoletti" and to the Dipartimento di Biotecnologie Mediche e Medicina Traslazionale, Università degli Studi di Milano.

CRediT authorship contribution statement

Antonucci Flavia: Supervision, Funding acquisition, Formal analysis. **Cambria Clara:** Investigation. **Scheggia Diego:** Supervision, Funding acquisition, Formal analysis. **Vandermeulen Lina:** Investigation. **Di Luca Monica:** Writing – review & editing, Funding acquisition. **Zianni Elisa:** Investigation. **Norata Giuseppe Danilo:** Writing – original draft, Funding acquisition, Conceptualization. **Musardo Stefano:** Investigation. **Roda Silvia:** Investigation. **Pelucchi Silvia:** Investigation, Funding acquisition, Formal analysis, Conceptualization. **Marcello Elena:** Writing – original draft, Funding acquisition, Conceptualization. **Bonacina Fabrizia:** Investigation, Funding acquisition. **Nasini Sofia:** Investigation. **Da Dalt Lorenzo:** Investigation, Formal analysis, Conceptualization. **Lupo Maria Giovanna:** Investigation. **De Cesare Giulia:** Investigation, Formal analysis, Conceptualization. **Ferri Nicola:** Supervision, Funding acquisition. **Stringhi Ramona:** Investigation. **Comai Stefano:** Supervision, Funding acquisition, Formal analysis. **D'Andrea Laura:** Investigation. **Gardoni Fabrizio:** Writing – review &

editing. **La Greca Filippo:** Investigation.

Declaration of Competing Interest

The authors declare that they have no known competing financial interests or personal relationships that could have appeared to influence the work reported in this paper.

Acknowledgment

We thank Annalisa Longhi for her technical assistance and Alessia Valente for her excellent practical work.

Appendix A. Supporting information

Supplementary data associated with this article can be found in the online version at doi:10.1016/j.phrs.2025.107652.

Data availability

Data will be made available on request.

References

[1] D. Li, J. Zhang, Q. Liu, Brain cell type-specific cholesterol metabolism and implications for learning and memory, Trends Neurosci. 45 (2022) 401–414, https://doi.org/10.1016/j.tins.2022.01.002.
[2] A. Linetti, A. Fratangeli, E. Taverna, P. Valnegri, M. Francolini, V. Cappello, M. Matteoli, M. Passafaro, P. Rosa, Cholesterol reduction impairs exocytosis of synaptic vesicles, J. Cell Sci. 123 (2010) 595–605, https://doi.org/10.1242/jcs.060681.
[3] Q. Liu, J. Trotter, J. Zhang, M.M. Peters, H. Cheng, J. Bao, X. Han, E.J. Weeber, G. Bu, Neuronal LRP1 knockout in adult mice leads to impaired brain lipid metabolism and progressive, age-dependent synapse loss and neurodegeneration, J. Neurosci. 30 (2010) 17068–17078, https://doi.org/10.1523/JNEUROSCI.4067-10.2010.
[4] Q. Liu, C.V. Zerbinatti, J. Zhang, H.-S. Hoe, B. Wang, S.L. Cole, J. Herz, L. Muglia, G. Bu, Amyloid precursor protein regulates brain apolipoprotein E and cholesterol metabolism through lipoprotein receptor LRP1, Neuron 56 (2007) 66–78, https://doi.org/10.1016/j.neuron.2007.08.008.
[5] M. Gliozzi, V. Musolino, F. Bosco, M. Scicchitano, F. Scarano, S. Nucera, M.C. Zito, S. Ruga, C. Carresi, R. Macrì, L. Guarnieri, J. Maiuolo, A. Tavernese, A. R. Coppoletta, C. Nicita, R. Mollace, E. Palma, C. Muscoli, C. Belzung, V. Mollace, Cholesterol homeostasis: researching a dialogue between the brain and peripheral tissues, Pharm. Res. 163 (2021) 105215, https://doi.org/10.1016/j.phrs.2020.105215.
[6] J. Zhang, Q. Liu, Cholesterol metabolism and homeostasis in the brain, Protein Cell 6 (2015) 254–264, https://doi.org/10.1007/s13238-014-0131-3.
[7] C.N. Barber, D.M. Raben, Lipid metabolism crosstalk in the brain: glia and neurons, Front. Cell Neurosci. 13 (2019), https://doi.org/10.3389/fncel.2019.00212.
[8] U. Jin, S.J. Park, S.M. Park, Cholesterol metabolism in the brain and its association with Parkinson's Disease, Exp. Neurobiol. 28 (2019) 554–567, https://doi.org/10.5607/en.2019.28.5.554.
[9] C. Lane-Donovan, W.M. Wong, M.S. Durakoglugil, C.R. Wasser, S. Jiang, X. Xian, J. Herz, Genetic restoration of plasma ApoE improves cognition and partially restores synaptic defects in ApoE-deficient mice, J. Neurosci. 36 (2016) 10141–10150, https://doi.org/10.1523/JNEUROSCI.1054-16.2016.
[10] C. Lane-Donovan, G.T. Philips, J. Herz, More than cholesterol transporters: lipoprotein receptors in CNS function and neurodegeneration, Neuron 83 (2014) 771–787, https://doi.org/10.1016/j.neuron.2014.08.005.
[11] U. Beffert, P.C. Stolt, J. Herz, Functions of lipoprotein receptors in neurons, J. Lipid Res. 45 (2004) 403–409, https://doi.org/10.1194/jlr.R300017-JLR200.
[12] M.D. Shapiro, H. Tavori, S. Fazio, PCSK9, Circ. Res. 122 (2018) 1420–1438, https://doi.org/10.1161/CIRCRESAHA.118.311227.
[13] A. Mullard, Nine paths to PCSK9 inhibition, Nat. Rev. Drug Discov. 16 (2017) 299–301, https://doi.org/10.1038/nrd.2017.83.
[14] M.S. Sabatine, PCSK9 inhibitors: clinical evidence and implementation, Nat. Rev. Cardiol. 16 (2019) 155–165, https://doi.org/10.1038/s41569-018-0107-8.
[15] G.D. Norata, G. Tibolla, A.L. Catapano, Targeting PCSK9 for Hypercholesterolemia, Annu Rev. Pharm. Toxicol. 54 (2014) 273–293, https://doi.org/10.1146/annurev-pharmtox-011613-140025.
[16] G.D. Norata, H. Tavori, A. Pirillo, S. Fazio, A.L. Catapano, Biology of proprotein convertase subtilisin kexin 9: beyond low-density lipoprotein cholesterol lowering, Cardiovasc Res. 112 (2016) 429–442, https://doi.org/10.1093/cvr/cvw194.
[17] N. Seidah, G. Mayer, A. Zaid, E. Rousselet, N. Nassoury, S. Poirier, R. Essalmani, A. Prat, The activation and physiological functions of the proprotein convertases, Int. J. Biochem. Cell Biol. 40 (2008) 1111–1125, https://doi.org/10.1016/j.biocel.2008.01.030.
[18] M. Abifadel, M. Varret, J.-P. Rabès, D. Allard, K. Ouguerram, M. Devillers, C. Cruaud, S. Benjannet, L. Wickham, D. Erlich, A. Derré, L. Villéger, M. Farnier, I. Beucler, E. Bruckert, J. Chambaz, B. Chanu, J.-M. Lecerf, G. Luc, P. Moulin, J. Weissenbach, A. Prat, M. Krempf, C. Junien, N.G. Seidah, C. Boileau, Mutations in PCSK9 cause autosomal dominant hypercholesterolemia, Nat. Genet. 34 (2003) 154–156, https://doi.org/10.1038/ng1161.
[19] J. Cohen, A. Pertsemlidis, I.K. Kotowski, R. Graham, C.K. Garcia, H.H. Hobbs, Low LDL cholesterol in individuals of African descent resulting from frequent nonsense mutations in PCSK9, Nat. Genet. 37 (2005) 161–165, https://doi.org/10.1038/ng1509.
[20] L. Tokgözoğlu, G.D. Norata, ORION-8: one step closer to understanding the safety and efficacy of inclisiran, Cardiovasc Res. 120 (2024) 1365–1366, https://doi.org/10.1093/cvr/cvae166.
[21] A.L. Catapano, A. Pirillo, G.D. Norata, New pharmacological approaches to target PCSK9, Curr. Atheroscler. Rep. 22 (2020) 24, https://doi.org/10.1007/s11883-020-00847-7.
[22] N.G. Seidah, A. Prat, A. Pirillo, A.L. Catapano, G.D. Norata, Novel strategies to target proprotein convertase subtilisin kexin 9: beyond monoclonal antibodies, Cardiovasc Res. 115 (2019) 510–518, https://doi.org/10.1093/cvr/cvz003.
[23] L. Da Dalt, L. Castiglioni, A. Baragetti, M. Audano, M. Svecla, F. Bonacina, S. Pedretti, P. Uboldi, P. Benzoni, F. Giannetti, A. Barbuti, F. Pellegatta, S. Indino, E. Donetti, L. Sironi, N. Mitro, A.L. Catapano, G.D. Norata, PCSK9 deficiency rewires heart metabolism and drives heart failure with preserved ejection fraction, Eur. Heart J. 42 (2021) 3078–3090, https://doi.org/10.1093/eurheartj/ehab431.
[24] L. Da Dalt, M. Ruscica, F. Bonacina, G. Balzarotti, A. Dhyani, E. Di Cairano, A. Baragetti, L. Arnaboldi, S. De Metrio, F. Pellegatta, L. Grigore, M. Botta, C. Macchi, P. Uboldi, C. Perego, A.L. Catapano, G.D. Norata, PCSK9 deficiency reduces insulin secretion and promotes glucose intolerance: the role of the low-density lipoprotein receptor, Eur. Heart J. 40 (2019) 357–368, https://doi.org/10.1093/eurheartj/ehy357.
[25] N.G. Seidah, S. Benjannet, L. Wickham, J. Marcinkiewicz, S.B. Jasmin, S. Stifani, A. Basak, A. Prat, M. Chrétien, The secretory proprotein convertase neural apoptosis-regulated convertase 1 (NARC-1): liver regeneration and neuronal differentiation, Proc. Natl. Acad. Sci. 100 (2003) 928–933, https://doi.org/10.1073/pnas.0335507100.
[26] K. Kysenius, P. Muggalla, K. Mätlik, U. Arumäe, H.J. Huttunen, PCSK9 regulates neuronal apoptosis by adjusting ApoER2 levels and signaling, Cell. Mol. Life Sci. 69 (2012) 1903–1916, https://doi.org/10.1007/s00018-012-0977-6.
[27] E. Rousselet, J. Marcinkiewicz, J. Kriz, A. Zhou, M.E. Hatten, A. Prat, N.G. Seidah, PCSK9 reduces the protein levels of the LDL receptor in mouse brain during development and after ischemic stroke, J. Lipid Res. 52 (2011) 1383–1391, https://doi.org/10.1194/jlr.M014118.
[28] S. Poirier, G. Mayer, S. Benjannet, E. Bergeron, J. Marcinkiewicz, N. Nassoury, H. Mayer, J. Nimpf, A. Prat, N.G. Seidah, The proprotein convertase PCSK9 induces the degradation of low density lipoprotein receptor (LDLR) and its closest family members VLDLR and ApoER2, J. Biol. Chem. 283 (2008) 2363–2372, https://doi.org/10.1074/jbc.M708098200.
[29] M. Liu, G. Wu, J. Baysarowich, M. Kavana, G.H. Addona, K.K. Bierilo, J.S. Mudgett, G. Pavlovic, A. Sitlani, J.J. Renger, B.K. Hubbard, T.S. Fisher, C.V. Zerbinatti, PCSK9 is not involved in the degradation of LDL receptors and BACE1 in the adult mouse brain, J. Lipid Res. 51 (2010) 2611–2618, https://doi.org/10.1194/jlr.M006635.
[30] E.M. O'Connell, F.W. Lohoff, Proprotein convertase subtilisin/kexin type 9 (PCSK9) in the brain and relevance for neuropsychiatric disorders, Front. Neurosci. 14 (2020), https://doi.org/10.3389/fnins.2020.00609.
[31] F. Zimetti, P. Caffarra, N. Ronda, E. Favari, M.P. Adorni, I. Zanotti, F. Bernini, F. Barocco, M. Spallazzi, D. Galimberti, C. Ricci, M. Ruscica, A. Corsini, N. Ferri, Increased PCSK9 cerebrospinal fluid concentrations in Alzheimer's Disease, J. Alzheimer'S. Dis. 55 (2016) 315–320, https://doi.org/10.3233/JAD-160411.
[32] H. Courtemanche, E. Bigot, M. Pichelin, B. Guyomarch, C. Boutoleau-Bretonnière, C. Le May, P. Derkinderen, B. Cariou, PCSK9 concentrations in cerebrospinal fluid are not specifically increased in Alzheimer's Disease, J. Alzheimer'S. Dis. 62 (2018) 1519–1525, https://doi.org/10.3233/JAD-170993.
[33] M.P. Adorni, M. Ruscica, N. Ferri, F. Bernini, F. Zimetti, Proprotein convertase subtilisin/Kexin Type 9, brain cholesterol homeostasis and potential implication for Alzheimer's Disease, Front. Aging Neurosci. 11 (2019), https://doi.org/10.3389/fnagi.2019.00120.
[34] P. Guedeney, G. Giustino, S. Sorrentino, B.E. Claessen, A. Camaj, D.N. Kalkman, B. Vogel, S. Sartori, S. De Rosa, U. Baber, C. Indolfi, G. Montalescot, G.D. Dangas, R.S. Rosenson, S.J. Pocock, R. Mehran, Efficacy and safety of alirocumab and evolocumab: a systematic review and meta-analysis of randomized controlled trials, Eur. Heart J. 43 (2022) e17–e25, https://doi.org/10.1093/eurheartj/ehz430.
[35] M.S. Sabatine, R.P. Giugliano, A.C. Keech, N. Honarpour, S.D. Wiviott, S. A. Murphy, J.F. Kuder, H. Wang, T. Liu, S.M. Wasserman, P.S. Sever, T.R. Pedersen, Evolocumab and clinical outcomes in patients with cardiovascular disease, N. Engl. J. Med. 376 (2017) 1713–1722, https://doi.org/10.1056/NEJMoa1615664.
[36] A. Marku, L. Da Dalt, A. Galli, N. Dule, P. Corsetto, A.M. Rizzo, A. Moregola, P. Uboldi, F. Bonacina, P. Marciani, M. Castagna, A.L. Catapano, G.D. Norata, C. Perego, Pancreatic PCSK9 controls the organization of the β-cell secretory pathway via LDLR-cholesterol axis, Metabolism 136 (2022) 155291, https://doi.org/10.1016/j.metabol.2022.155291.
[37] B.G. Kim, H.N. Dai, M. McAtee, S. Vicini, B.S. Bregman, Labeling of dendritic spines with the carbocyanine dye DiI for confocal microscopic imaging in lightly fixed cortical slices, J. Neurosci. Methods 162 (2007) 237–243, https://doi.org/10.1016/J.JNEUMETH.2007.01.016.

[38] S. Pelucchi, L. Vandermeulen, L. Pizzamiglio, B. Aksan, J. Yan, A. Konietzny, E. Bonomi, B. Borroni, A. Padovani, M.B. Rust, D. Di Marino, M. Mikhaylova, D. Mauceri, F. Antonucci, V. Edefonti, F. Gardoni, M. Di Luca, E. Marcello, Cyclase-associated protein 2 dimerization regulates cofilin in synaptic plasticity and Alzheimer's disease, Brain Commun. 2 (2020), https://doi.org/10.1093/BRAINCOMMS/FCAA086.

[39] L. Da Dalt, A. Moregola, M. Svecla, S. Pedretti, F. Fantini, M. Ronzio, P. Uboldi, D. Dolfini, E. Donetti, A. Baragetti, N. Mitro, L. Scorrano, G.D. Norata, The inhibition of inner mitochondrial fusion in hepatocytes reduces NAFL and improves metabolic profile during obesity by modulating bile acid conjugation, Cardiovasc Res. (2023), https://doi.org/10.1093/cvr/cvad169.

[40] L. D'Andrea, M. Audano, S. Pedretti, S. Pelucchi, R. Stringhi, G. Imperato, G. De Cesare, C. Cambria, M.H. Laporte, N. Zamboni, F. Antonucci, M. Di Luca, N. Mitro, E. Marcello, Glucose-derived glutamate drives neuronal terminal differentiation in vitro, EMBO Rep. (2024), https://doi.org/10.1038/s44319-023-00048-8.

[41] M.C. Dinamarca, F. Guzzetti, A. Karpova, D. Lim, N. Mitro, S. Musardo, M. Mellone, E. Marcello, J. Stanic, T. Samaddar, A. Burguière, A. Caldarelli, A.A. Genazzani, J. Perroy, L. Fagni, P.L. Canonico, M.R. Kreutz, F. Gardoni, M. Di Luca, Ring finger protein 10 is a novel synaptonuclear messenger encoding activation of NMDA receptors in hippocampus, ELife 5 (2016) e12430, https://doi.org/10.7554/eLife.12430.

[42] J. Miao, P.V. Manthena, M.E. Haas, A.V. Ling, D.-J. Shin, M.J. Graham, R. M. Crooke, J. Liu, S.B. Biddinger, Role of insulin in the regulation of proprotein convertase subtilisin/Kexin type 9, Arterioscler. Thromb. Vasc. Biol. 35 (2015) 1589–1596, https://doi.org/10.1161/ATVBAHA.115.305688.

[43] G.R.I. Barker, E.C. Warburton, When is the hippocampus involved in recognition memory? J. Neurosci. 31 (2011) 10721–10731, https://doi.org/10.1523/JNEUROSCI.6413-10.2011.

[44] X. Wang, C. Zhang, G. Szábo, Q.-Q. Sun, Distribution of CaMKIIα expression in the brain in vivo, studied by CaMKIIα-GFP mice, Brain Res. 1518 (2013) 9–25, https://doi.org/10.1016/j.brainres.2013.04.042.

[45] J.Z. Tsien, D.F. Chen, D. Gerber, C. Tom, E.H. Mercer, D.J. Anderson, M. Mayford, E.R. Kandel, S. Tonegawa, Subregion- and cell type–restricted gene knockout in mouse brain, Cell 87 (1996) 1317–1326, https://doi.org/10.1016/S0092-8674(00)81826-7.

[46] Y. Chen, U. Beffert, M. Ertunc, T.-S. Tang, E.T. Kavalali, I. Bezprozvanny, J. Herz, Reelin modulates NMDA receptor activity in cortical neurons, J. Neurosci. 25 (2005) 8209–8216, https://doi.org/10.1523/JNEUROSCI.1951-05.2005.

[47] G. Lavezzari, J. McCallum, R. Lee, K.W. Roche, Differential binding of the AP-2 adaptor complex and PSD-95 to the C-terminus of the NMDA receptor subunit NR2B regulates surface expression, Neuropharmacology 45 (2003) 729–737, https://doi.org/10.1016/S0028-3908(03)00308-3.

[48] I. Björkhem, D. Lütjohann, U. Diczfalusy, L. Ståhle, G. Ahlborg, J. Wahren, Cholesterol homeostasis in human brain: turnover of 24S-hydroxycholesterol and evidence for a cerebral origin of most of this oxysterol in the circulation, J. Lipid Res. 39 (1998) 1594–1600.

[49] D.H. Mauch, K. Nägler, S. Schumacher, C. Göritz, E.-C. Müller, A. Otto, F. W. Pfrieger, CNS synaptogenesis promoted by glia-derived cholesterol, Science (1979) 294 (2001) 1354–1357, https://doi.org/10.1126/science.294.5545.1354.

[50] H. Hering, C.-C. Lin, M. Sheng, Lipid rafts in the maintenance of synapses, dendritic spines, and surface AMPA receptor stability, J. Neurosci. 23 (2003) 3262–3271, https://doi.org/10.1523/JNEUROSCI.23-08-03262.2003.

[51] A. Barco, J.M. Alarcon, E.R. Kandel, Expression of constitutively active CREB protein facilitates the late phase of long-term potentiation by enhancing synaptic capture, Cell 108 (2002) 689–703, https://doi.org/10.1016/S0092-8674(02)00657-8.

[52] S. Poirier, A. Prat, E. Marcinkiewicz, J. Paquin, B.P. Chitramuthu, D. Baranowski, B. Cadieux, H.P.J. Bennett, N.G. Seidah, Implication of the proprotein convertase NARC-1/PCSK9 in the development of the nervous system, J. Neurochem. 98 (2006) 838–850, https://doi.org/10.1111/j.1471-4159.2006.03928.x.

[53] A. Pärn, D. Olsen, J. Tuvikene, M. Kaas, E. Borisova, M. Bilgin, M. Elhauge, J. Vilstrup, P. Madsen, M.C. Ambrozkiewicz, R.U. Goz, T. Timmusk, V. Tarabykin, C. Gustafsen, S. Glerup, PCSK9 deficiency alters brain lipid composition without affecting brain development and function, Front. Mol. Neurosci. 15 (2023), https://doi.org/10.3389/fnmol.2022.1084633.

[54] C. Sala, M. Segal, Dendritic spines: the locus of structural and functional plasticity, Physiol. Rev. (2014), https://doi.org/10.1152/physrev.00012.2013.

[55] Y.Z. Şener, L. Tokgözoğlu, Pleiotropy of PCSK9: functions in extrahepatic tissues, Curr. Cardiol. Rep. 25 (2023) 979–985, https://doi.org/10.1007/s11886-023-01918-2.

[56] K.R. Tovar, G.L. Westbrook, The Incorporation of NMDA receptors with a distinct subunit composition at nascent hippocampal synapses *in vitro*, J. Neurosci. 19 (1999) 4180–4188, https://doi.org/10.1523/JNEUROSCI.19-10-04180.1999.

[57] L. Liu, T.P. Wong, M.F. Pozza, K. Lingenhoehl, Y. Wang, M. Sheng, Y.P. Auberson, Y.T. Wang, Role of NMDA receptor subtypes in governing the direction of hippocampal synaptic plasticity, Science (1979) 304 (2004) 1021–1024, https://doi.org/10.1126/science.1096615.

[58] M.J. Kim, A.W. Dunah, Y.T. Wang, M. Sheng, Differential roles of NR2A- and NR2B-containing NMDA receptors in Ras-ERK signaling and AMPA receptor trafficking, Neuron 46 (2005) 745–760, https://doi.org/10.1016/j.neuron.2005.04.031.

[59] S.S. Reddy, T.E. Connor, E.J. Weeber, W. Rebeck, Similarities and differences in structure, expression, and functions of VLDLR and ApoER2, Mol. Neurodegener. 6 (2011) 30, https://doi.org/10.1186/1750-1326-6-30.

[60] E.J. Weeber, U. Beffert, C. Jones, J.M. Christian, E. Förster, J.D. Sweatt, J. Herz, Reelin and ApoE receptors cooperate to enhance hippocampal synaptic plasticity and learning, J. Biol. Chem. 277 (2002) 39944–39952, https://doi.org/10.1074/jbc.M205147200.

[61] S.B. Dumanis, H.-J. Cha, J.M. Song, J.H. Trotter, M. Spitzer, J.-Y. Lee, E.J. Weeber, R.S. Turner, D.T.S. Pak, G.W. Rebeck, H.-S. Hoe, ApoE receptor 2 regulates synapse and dendritic spine formation, PLoS One 6 (2011) e17203, https://doi.org/10.1371/journal.pone.0017203.